Altered viscoelastic properties of the *Nicotiana tabacum* BY-2 suspension cell lines adapted to high concentrations of NaCl and mannitol

Tomasz Skrzypczak[1], Mikołaj Pochylski[2], Magdalena Rapp[3], Przemysław Wojtaszek[4], Anna Kasprowicz-Maluśki[4]

[1] Center for Advanced Technologies, Adam Mickiewicz University, Poznan, Poland

[2] Faculty of Physics, Adam Mickiewicz University, Poznan, Poland

[3] Faculty of Chemistry, Adam Mickiewicz University, Poznan, Poland

[4] Department of Molecular and Cellular Biology, Institute of Molecular Biology and Biotechnology, Adam Mickiewicz University, Poznan, Poland

Abstract

Plant cells have to maintain the cellular microenvironment within a certain range of its properties to stay alive and grow. The functioning of the cell requires a continuous exchange of mass and energy with an environment. Such system openness could lead to perturbation in cellular microenvironment and disorder in molecular processes. Hyperosmolarity significantly stresses cells, induces ROS, promotes water efflux, and decreases turgor, optionally up to plasmolysis and a cell's shrinkage. However, in time upon exposure to osmotic stress a cellular adaptation could be developed. How the biomechanical balance of the cell is established and maintained in an environment of osmotic stress remains a nurturing question. We show that changes of the viscoelastic properties of protoplasts are element of such adaptation.

We used Brillouin light scattering (BLS) and BODIPY-based fluorescence molecular rotors to study *Nicotiana tabacum* suspension BY-2 cells adapted to high concentrations of NaCl and mannitol. We revealed an increased molecular crowd and viscoelasticity in adapted BY-2 cells, as well as an altered plasma membrane tension. Importantly, viscosity-related changes imposed on adapted BY-2 cells by salt stress were smaller than those observed for control cells. Cellular microenvironments were elucidated in on the background of their own environments, what revealed that alterations of cytoplasm and vacuoles viscoelasticity in adapted cells has also a relative dimension.

This work provides the first semi-quantitative data, to our knowledge, for viscoelastic cellular changes in plant cells adapted to growth under salt and osmotic stress conditions and exposed to subsequent short-term stress. Applied methods provide evidence that adaptation to hyperosmotic stress leads to different ratio in the protoplast and environment qualities that helps to maintain cell integrity. Many challenges remain in the field of plant mechanobiology, to which our approach could provide valuable insight into plant cell responses to the environment and the further development of useful methods.

Introduction

Understanding of the interactions between cellular microenvironment and the external environment remains a significant challenge in cell biology. One fundamental environmental factor with pleiotropic impacts is osmolarity, which can alter water activity and directly affect all cellular processes and biomechanics of a plants cell (Watson et al., 2023; Zonia & Munnik, 2007). Despite the vast information on the response to stress, it is still elusive how much changes in the properties of biophysical cells originate from the direct impact of an environment (i.e. passively imposed), and from the activity of cells in response to stress. Hyperosmolarity, as well as desiccation and temperature fluctuations, could severely altered water activity in cells, what disturbs cell growth, and whole

molecular machinery, which enforces reaction to overcome dysfunctions (Romero-Perez et al., 2023; van Zelm et al., 2020; Watson et al., 2023; Zonia & Munnik, 2007). Recent studies have demonstrated that hyperosmolarity stress rapidly increases also cellular viscosity and molecular crowd in neuroblastoma cells (Kitamura et al., 2023). In the case of salt stress, an excessive concentration of sodium adds further toxicity by altering cation homeostasis (K^+/Na^+) and plasma membrane potential (Li & Yang, 2023). Also, a high concentration of chloride anion is toxic and disturb anions homeostasis and consequently organellar physiology (Geilfus, 2018). Fundamentally, hyperosmotic stress explicitly leads to increased molecular crowd (MC), due to water efflux, that dramatically altered conditions, that are crucial for cellular molecular machinery (Romero-Perez et al., 2023). Moreover, a quick water efflux from a cell could induce temporal or irreversible plasmolysis. During osmotic and salt stress at first signalling pathways are activated, leading to quick stress response, in time cells adjust their physiology, what include growth quiescence and recovery (reviewed in Julkowska & Testerink, 2015; Zhu, 2002). With prolonged increased salinity, plants could develop adaptations at the cellular level, that include increased biosynthesis of osmolytes, alteration of cell walls structure, and intense export of Na^+ to vacuoles (Flowers & Colmer, 2015; Li & Yang, 2023; van Zelm et al., 2020; Zhao et al., 2020). The viscosity, that also could change due to hyperosmolarity, was shown to directly impact metabolism and enzymatic reactions (Gavish & Werber, 1979; Kitamura et al., 2023; Uribe & Sampedro, 2003). However, the viscoelastic properties of cells, although being crucial realms in cells interactions with an environment, are much less studied than networks of signalling pathways and transcriptional response. It was shown, that in mammalian cells, cytoplasm behaves differently depending on molecules size, like liquid or like a gel. Moreover, cytoplasmic viscosities were found as similar across various cells lines (Kwapiszewska et al., 2020). A reason that local viscosity and MC have to be kept in a certain range is clearing the path for efficient diffusion (Alfano et al., 2023). In yeasts, it was shown that 'viscoadaptation' depends on the synthesis of glycogen and trehalose. Importantly, 'viscoadaptation' allows yeast cells to maintain efficient diffusion in a wide temperature range (Persson et al., 2020). In HeLa cells, changes in cells volumes in response to osmotic shocks are followed by changes in membrane tensions, and such volume-membrane tension dynamics is actively regulated by a cell (Roffay et al., 2021). Recently, it was shown, that fundamentally for the stress response, biocondensates made of Intrinsically Disordered Proteins (IPDs) counteract microenvironmental instabilities induced by temperature and osmolarity changes (Watson et al., 2023).

In the last decade many techniques have been developed and utilised to measure mechanical properties of living biological materials, which enable *in situ* measurements (Elsayad et al., 2016; Farokh Payam & Passian, 2024; Kitamura et al., 2023; Michels et al., 2020; Robinson et al., 2023; Seelbinder et al., 2024; P.-H. Wu et al., 2018). Cell microenvironment-sensing dyes based on fluorescence lifetime (FLIM) signals have proven their robustness, independence from concentration, precision in revealing cellular characteristics, such as pH, intrinsically disordered proteins status, redox status, hormone concentrations, and biomechanical parameters, such as viscosity and ionic strength as well (Colin et al., 2022; Cuevas-Velazquez et al., 2021; Kitamura et al., 2023; Koveal et al., 2020; Michels et al., 2020; Miller et al., 2020; Steinbeck et al., 2020; van der Linden et al., 2021).

Turgor pressure and the bulk elastic modulus of a plant cell can be measured directly with a microcapillary invasive pressure probe (Tomos & Leigh, 1999). Less-invasive approach for measuring elastic and viscoelastic properties of plant cells are indentation methods, based on the idea of measuring the force required to displace the surface of a sample by a given distance. The resulting force versus indentation curves can then be used to calculate the stiffness of a sample. These include atomic force microscopy (AFM) (Milani et al., 2011; Peaucelle et al., 2011; Sampathkumar et al., 2014), cellular force microscopy (CFM) (Routier-Kierzkowska et al., 2012), microcompression (Wang, 2004; Wang et al., 2006), and other single-point indentation systems (Hayot et al., 2012; Lintilhac et al., 2000).

Introduction of BLS (Brillouin Light Scattering) as an all-optical contactless mechanical probe with diffraction-limited spatial resolution was greeted with enthusiasm. This technique can deliver mechanical information when physical access to the region of interest cannot be gained, such as in a cell or multicellular object (Elsayad et al., 2016; Gouveia et al., 2019; Margueritat et al., 2019; Roberts et al., 2021; Wisniewski et al., 2020). The very significant property of interest in biomechanics is Young's modulus, which quantifies the amount of deformation of a material subjected to uniaxial stress. In classical mechanical testing, the stress (or deformation) needs to be applied by means of external stimulus. As a result, most of the classical techniques for mechanical testing suffer from the same flaw, namely the necessity of direct contact with the sample. This strongly hinders the mechanical testing of samples where such direct contact is often very limited. Brillouin microscopy has been constantly developed over time to overcome limitations of the methods and adjust/fit it to the requirements of analysis with living samples. Cellular resolution of living samples was shown with Brillouin microscopy in 2016 (Bevilacqua et al., 2023; Elsayad et al., 2016). Recently, the method was also used to study the stiffness of the cell walls of plants at the cellular level in roots of *Arabidopsis thaliana* (Bacete et al., 2022; McKenna et al., 2019). Although the application of Brillouin microscopy might allow determination of the *elastic factor* of a solid body, in soft matter/hydrated materials, such as cells or polymers solutions, the water content might be more reliably measured (P. J. Wu et al., 2018). BLS was also revealed as an efficient tool for investigating molecular crowd dynamics in multicellular spheroids in response to hyperosmolarity (Yan et al., 2021).

Tobacco (*Nicotiana tabacum*) BY-2 suspension roots cell line is a well-established model in cell biology and biotechnology research (Hoque et al., 2007; Jelínková et al., 2015; Khatun et al., 2020; Kurusu et al., 2012; Olmos et al., 2017a; Srba et al., 2016). Utilization of BY-2 allows for investigation of cells derived from relatively homogenous population, that live in the homogenous environment (culture media). Here, we utilised BY-2 cell lines that were adapted to high concentrations of NaCl and mannitol. Gradual adaptations were performed as far as the highest tolerated concentrations were obtained, i.e. 190 mM NaCl for NaCl adapted BY-2 (BY-2:NaCl), and 450 mM mannitol for mannitol adapted BY-2 (BY-2:Mann). The adapted cell lines obtained have survived for multiple generations. The adapted cell lines presented significantly different morphologies and transcriptomes from the control cell lines and from each other as well (Skrzypczak et al., 2024).

Here, we present results of investigation on viscoelastic properties of *Nicotiana tabacum* suspension BY-2 cells under various osmotic conditions. The utilisation of BODIPY(BDP)-based molecular rotors and BLS enables us to reveal viscoelastic BY-2 properties with subcellular precision and non-cells destructive methods. Moreover, for the first time, we show the utilisation of BLS to study the plant protoplasts in a reference to mechanical properties of an environment.

Materials and methods

BY-2 cultures

Tobacco BY-2 suspension-cultured cells were maintained in liquid medium, pH 5.0, containing Murashige and Skoog salts (Murashige & Skoog 1962) and (per litre): 30 g sucrose, 100 mg inositol, 3 mg 2,4-D, 370 mg KH_2PO_4 and 1 mg thiamine-HCl (Nagata *et al.* 1992). Cells were subcultured weekly at 10 ml of culture per 70 ml of fresh medium in 300-mL Erlenmeyer flasks. Cultures were incubated at 21°C on a gyratory shaker at 120 rpm with a 2.5-cm displacement. During 18 months, cells were gradually adapted to grow in a medium supplemented with either 450 mM mannitol or 190 mM NaCl. The cultures were transferred to fresh media containing increasing concentration of mannitol or NaCl in sequential manner, starting with 50 mM mannitol and 20 mM NaCl (osmotic agents concentrations were increased every 2 months), but were otherwise handled identically to the control BY-2 cells. Immediately following transfer, the decreased intensity of cell divisions and decreased fresh weight of cells in culture were noted. However, after 4-8 subsequent passages, the adapted cells exhibited the

same growth properties as control ones. This was usually considered as the time point appropriate for the next step-increase in the osmotic agent concentration in culture media. Final concentrations of mannitol (450 mM) and NaCl (190 mM) were the highest that were not lethal to BY-2 cells. The osmolarities of fresh media were measured with an osmometer. The highest media osmolarity was measured in the high mannitol adapted line (BY-2:Mann; ~750 mOsm/kg), than in the high NaCl adapted line (BY-2:NaCl; ~550 mOsm/kg). The lowest osmolarity was measured for the standard BY-2 medium used to culture BY-2:Control; ~220 mOsm/kg .

All the results described herein are from cultures maintained in the presence of final concentrations of osmotic agents for at least 15 years, and all the sampling was done on the third day (logarithmic growth phase) after transfer to fresh medium. To improve synchronization, cultures were kept for 2 weeks without subculture, followed by dilution of 5 ml of old culture in 70 ml of fresh medium. Undifferentiated and dividing cells were observed 2 days after that subculture, while differentiated non-dividing cells were observed after 10 days of culture.

Mannitol and salt stress experiments were conducted in the middle days of the culture cycle. For stress experiments, NaCl and mannitol were added to medium derived by centrifugation from the same day of culture. This allowed for minimising effects of media composition different from those of stress agent.

Fluorescent Ph-BODIPY rotors synthesis

BODIPY-based (BDP) molecular rotors were synthesised according to a protocol described previously (Michels et al., 2020). Procedure and NMR data results of synthesised rotors are available in Supplement: SI_BDP_synthesis.pdf

BODIPY rotors imaging and data analysis

Cellular microviscosity was measured with BDP-based molecular rotor fluorescence probes in the middle days of culture cycles. Cells were incubated with PEG-BDP for 1 h and with N^+-BDP for 3 h, then washed twice with their respective culture media derived from a recent day of BY-2 culture. The PicoHarp300-Dual Channel SPAD system (PicoQuant) in combination with a Nikon A1Rsi microscope armed with the 20x dry or 60x /1.20 water immersion objective was used. The Picosecond Pulsed Diode Laser LDH-D-C-485 and Supercontinuum Tunable White Light Laser (488 nm) were used for generation of 100 ps excitation pulses at a repetition of 40 MHz. The images were of frame size of 256 × 256 pixels and were collected with an average count rate of around 10^5 photons per second for apprx. 30-60 s , that max photons per pixel reached 3 000 counts. FLIM data were collected from more than 30 cells. ROI were used to select properly stained subcellular compartments. Furthermore, also cells-free areas, but the surrounding area of the cells was used to obtain a real lifetime signal of the environment of BY-2 cells (media). The fluorescence decay curves were fit in each pixel with a two-component exponential decay, and the lifetime mean and SD were calculated. The lifetime signals distributions were assigned to 0.1 ns wide bins, then events occurrence scaled in (0, 1) range and plotted with matplotlib as histograms.

Brillouin light scattering

In the Brillouin light scattering (BLS) experiment the incident laser beam from laser (Spectra Physics, Excelsior, λ=532nm) was delivered to home-built microscope of the usual design (Fig.1a). The beam of vertical polarisation, reflected by the polarising beam-splitter, was passed through $\lambda/4$ to produce incident beam of circular polarisation. The beam was focused on the sample with a 20x microscope objective (Zeiss LD Achroplan Korr; NA=0.4). A low numerical aperture objective was used to reduce the spectral broadening effect (Antonacci et al., 2013) with the consequence of increasing the volume of scattering (6x20um). The sample was moved in the XY plane with a motorised translation stage (Märzhäuser Wetzlar GmbH & Co. KG). The power measured on the sample was 10 mW. The light

backscattered from the sample was collected by the same objective and after restoring the vertical polarization (by passing through λ/4) was transmitted by beam-splitter towards λ/2 used to rotate polarization plane of scattered light before focussing on the entrance pinhole of the Brillouin spectrometer. For Brillouin spectrum measurement, Tandem Fabry-Perot Interferometer (TFPI) (TFP2, The Table Stable Ltd.) whose spectral range (FSR) was set to 15 GHz (10 mm mirror spacing).

The sample was sandwiched between two microscope slides. The starting position for XY scanning was chosen after inspection of the sample using bright-field imaging with the same microscope. At given XY position, recorded spectrum was average of 15 spectral sweeps giving ~10s for single spectrum acquisition. Spectra were collected for a 16x16 grid spaced by 2 um. The total time to collect a single map was ~45min. Each map was measured for a fresh sample.

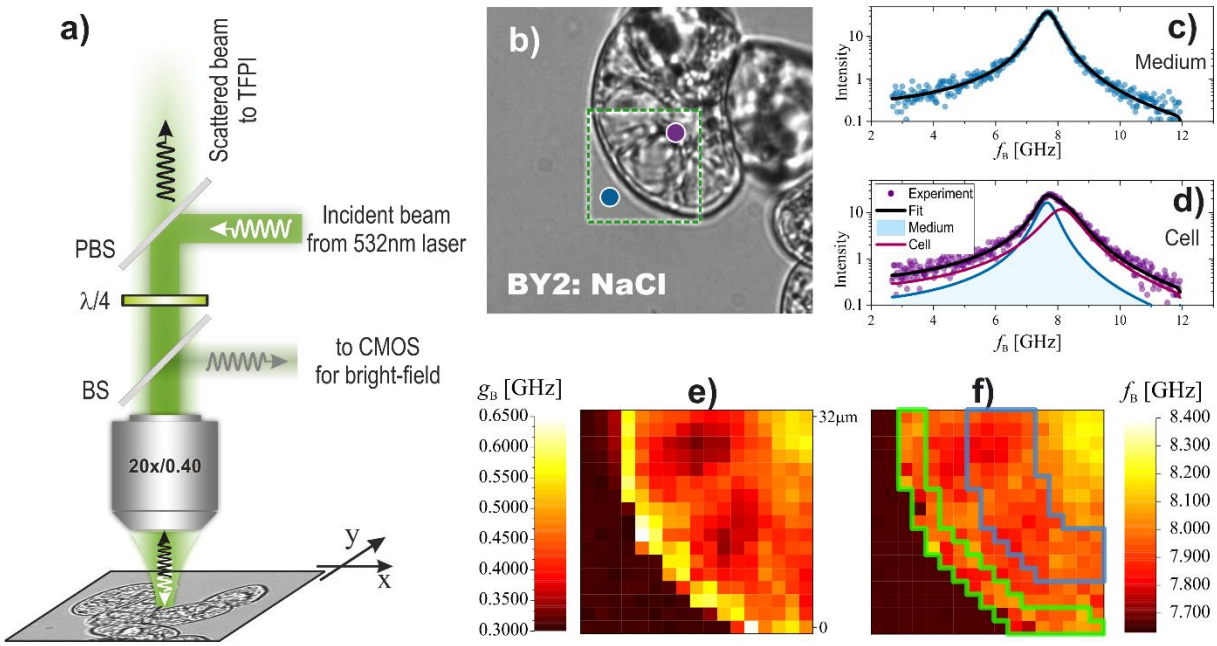

Fig. 1. Brillouin imaging of a cell. a) Schematic of the experimental setup for Brillouin micro-spectroscopy. BS, PBS, λ/4 and λ/2 stand, respectively, for removable beam splitter (for bright-field imaging), polarising beam splitter, quarter- and half-wave plates. b) Bright-field image of the cell. The green rectangle indicates the area chosen for Brillouin imaging. The blue and violet circles show the positions of the buffer and interior of the cell, respectively. c) Brillouin spectrum (anti-Stokes side) collected for buffer (Blue circle in b)). Notice that a single Brillouin peak is observed. d) Brillouin spectrum acquired inside the cell (violate circle in b)). Notice that the spectrum cannot be described by a single peak. Two peaks are necessary to reproduce the spectrum. One peak is assumed to come from scattering from a buffer (blue line). The second is a signal from the cell interior (dark red line). During spectrum fitting, the Brillouin peak parameters of the first peak were fixed to the values found for buffer. The Brillouin line shift and line width of the second peak (corresponding the cell) were mapped. e) Map of the Brillouin linewidth. f) map of the Brillouin lines shift. Green line border region identified in BF as cytoplasm dominating. Blue line border region identified in BF as vacuole dominating. The size of the maps is 32um.

In the investigation of cell mechanics, cells from every BY-2 line were extensively mapped, with more than 8 cells analysed for each line. The mapping process involved capturing bright field images to select specific regions showing bulk buffer, cell wall, and cell interior visibility, as illustrated in Fig.1b.

Brillouin spectra analysis was conducted for pixels corresponding to the bulk medium, employing a single-phase model (Eq.S1) to extract the values of fB, buffer, and gB, buffer, as shown in Fig.1c. Subsequently, the Brillouin spectra for the pixels corresponding to the cell interior and cell boundary (Fig.1d) were fitted using a two-phase model (Eq.S2). The parameters for the first Brillouin doublet were constrained to values obtained for the medium (fB,medium and gB,medium). The fitting process involved free parameters, including the second phase parameters (fB,cell and gB,cell) and the amplitude of the Brillouin peak of the medium (AB, medium), following a similar approach presented in a prior study (Mattana et al., 2018).

The spatial distribution of fB, cell, and gB, cell was visually represented in the form of maps (Fig.1e,f), allowing for a comprehensive understanding of their variations across the cell. To enhance the analytical depth, manual selection of pixels was performed in each map, identifying three distinct regions: 1) medium (cell exterior/environment), 2) vacuole (interior of the cell, excluding nuclear region), and 3) cytoplasm (a protoplast in a cell wall's vicinity).

Further insights into the viscoelastic properties of the cell and its environment were obtained through the production of histograms. The parameters of the Brillouin line, such as shift and width, were examined for the three identified regions, providing a statistical overview of cellular mechanics and its surrounding medium. This multifaceted approach not only enabled a detailed analysis of individual cells, but also contributed to a broader understanding of the viscoelastic characteristics across different BY-2 lines.

Brillouin spectra fitting

The Brillouin spectrum recorded from pure medium (Fig.1c) shows a single Brillouin line. To obtain the frequency shifts and linewidth, the spectra were fitted using hydrodynamic expression convoluted with the instrumental resolution function [Pecora].

$$I(f) = A_B\left[\frac{g_B}{(f+f_B)^2+g_B^2}+\frac{g_B}{(f-f_B)^2+g_B^2}\right]+ \frac{A_B g_B}{f_B}\left[\frac{f+f_B}{(f+f_B)^2+g_B^2}-\frac{f-f_B}{(f-f_B)^2+g_B^2}\right] \quad \text{(S1)}$$

In eq.S1 first two terms describe the Brillouin doublet composed of two lines symmetrically of amplitude AB shifted at fB, with the width (half width at half maximum) gB, whereas the last two terms ensure the preservation of the first moment sum rule and only affect the symmetry of the Brillouin doublet.

When the Brillouin signal was acquired from within the cell (Fig.1d), we found that Eq.S1 does not provide a proper description. When observed in logarithmic scale, the spectrum is clearly composed of two peaks. The spectra were fitted with the two-phase model (a sum of two Brillouin doublets) convolved with the instrumental resolution function of TFPI.

$$I(f) = \sum_{i=buffer,\text{cell}}\left\{A_{B,i}\left[\frac{g_{B,i}}{(f+f_{B,i})^2+g_{B,i}^2}+\frac{g_{B,i}}{(f-f_{B,iB})^2+g_{B,i}^2}\right]+ \frac{A_{B,i}g_{B,i}}{f_{B,i}}\left[\frac{f+f_{B,iB}}{(f+f_{B,i})^2+g_{B,i}^2}-\frac{f-f_{B,i}}{(f-f_{B,i})^2+g_{B,i}^2}\right]\right\} \quad \text{(S2)}$$

The meaning of the symbols in Eq.S2 is the same as for Eq.S1.

We found that the parameters (fB and gB) of one of these peaks correspond to those found for pure medium. Therefore, we interpret the spectra as being recorded from a two-phase system. One phase corresponds to the medium surrounding cell and the other to the cell itself. The reason we see the signal from both phases (buffer and cell) is low optical resolution of our system given by a low numerical aperture of the objective together with a high diameter of entrance pinhole (200um).

The existence of a Brillouin signal from the cell and from the buffer was previously observed in microspectroscopic experiments utilising TFPI (Mattana et al., 2018). It is known to deliver spectra of

exceptional quality and it is not clear if the same "buffer contamination" exists also in spectra recorded with VIPA spectrometers more commonly utilised by Brillouin imaging.

During fitting, the Brillouin line shape parameters for the buffer phase ($f_{B,medium}$ and $g_{B,medium}$) were kept constant and fixed to the value found from the fitting spectra acquired in pure buffer using eq.S1.

Results

Adapted BY-2 lines exhibited a higher cytoplasmic molecular crowd

Previously characterised, BDP-based cytoplasmic and plasma membrane (PM) based molecular rotors were used to obtain information on the viscosity of BY-2 subcellular compartments. The signals derived from PEG-BDP in the cytoplasm could be interpreted as an indicator of local molecular crowd (MC), while N^+-BDP works as a sensor of plasma membrane (PM) fluidity (Michels et al., 2020). In the media, that is, a liquid environment, PEG-BDP provides data that correspond to viscosity (Michels et al., 2020), so the cytoplasmic molecular crowd was presented on background of environmental viscosity.

PEG-BDP efficiently stained the cytoplasm of BY-2 cells and did not penetrate into vacuoles, but clearly diffused also to the nucleus (Fig. 2). ROIs were used to isolate signals from the cytoplasm and to exclude denser nuclear areas. Lifetime was also measured in the medium area in cells vicinity (~ 50-100 um from cells) to respect the impact of the real environment on the cellular microenvironment. This allowed the calculation relative to the medium the differences between cells and their environment (Δ). The lifetimes measured in the surrounding media were smaller than those found inside the cells, and the lifetime distributions of the media were clearly distinguishable from those of the cells (Table 1).

$$\text{Delta } (\Delta) = \frac{cytoplasm\ mean\ lifetime}{medium\ mean\ lifetime} - 1$$

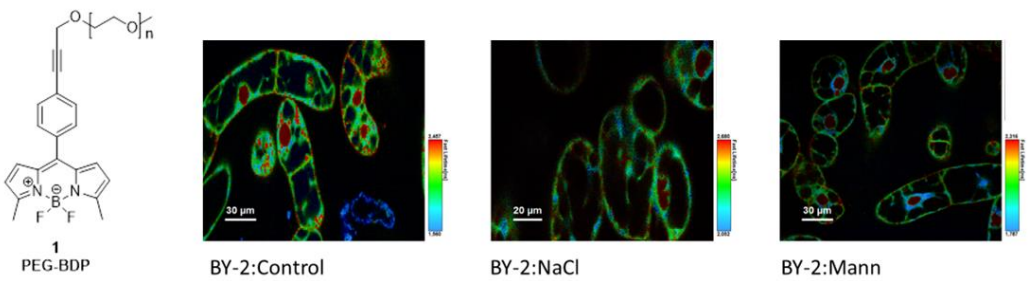

Fig. 2. PEG-BDP formula and images of PEG-BDP stained BY-2 lines. Lifetime BY-2 images are in false colour scale that represent the mean fluorescence lifetime for each pixel, expressed in nanoseconds. Nuclear regions with significantly higher lifetime values were not considered to obtain the cytoplasmic lifetime and molecular crowd.

Cells were expected to be denser and more vicious than surrounding media. Indeed, BY-2:Control exhibited a higher lifetime of PEG-BDP in the cytoplasm (mean lifetime 2.1 ns), than in the media (mean lifetime 1.69 ns), which showed a denser cytoplasm, than the surrounding medium. The relative to the medium difference (Δ) between the cytoplasm and the mean lifetime values of the media were 24% (Table 1).

The adaptation to medium of high osmolarity requires that cells counteract and preserve intracellular conditions that allow for efficient diffusion and balance of water flow between a cell and an environment. The adapted BY-2 lines displayed different PEG-BDP lifetime signals distributions, than BY-2:Control. Distributions of lifetime values were shifted toward higher lifetimes. The mean lifetime

values were 0.7-0.8 ns higher for adapted cell lines, than for BY-2:Control (Table 1). However, the relative to medium lifetime values (Δ) values are smaller in both adapted BY-2 lines than in BY-2:Control. Adapted cells lifetime signal distributions are closer to the media signals.

The relative lifetime (Δ) of PEG-BDP in the cytoplasm was the highest in BY-2:Control (24%), followed by BY-2:Mann (20%) and BY-2:NaCl (12%) (Table 1). This effect depended not only on cells derived signals, but also on varied media lifetimes, with the widest distribution for BY-2:NaCl medium and the narrowest for BY-2:Mann medium (Fig. 3). The medium composition had an impact on medium biomechanical properties. Moreover, cells also might modify properties of their surroundings by i.a. secretion or cell wall degradation.

A longer lifetime of PEG-BDP in adapted BY-2 implicates a more crowded cytoplasm, despite the fact that cells were not subjected to any osmotic stress and had been living in such conditions for many generations. While, the mean PEG-BDP lifetime of the adapted cell media is highest for BY-2:NaCl, it did not correspond to the measured media osmolarities, which was the highest for the BY-2:Mann media, not for the BY-2:NaCl media (Table 1). Because of the varied molecules' size and the electric charges, mannitol and NaCl might differently affect the osmolarity and viscosity of the medium. In two different environments of high osmolarity altered cytoplasmic MC were observed. Such cells properties correlate with long term suspension cell cultures survival and growth in high NaCl and mannitol, and might be considered as element of osmoadaptation.

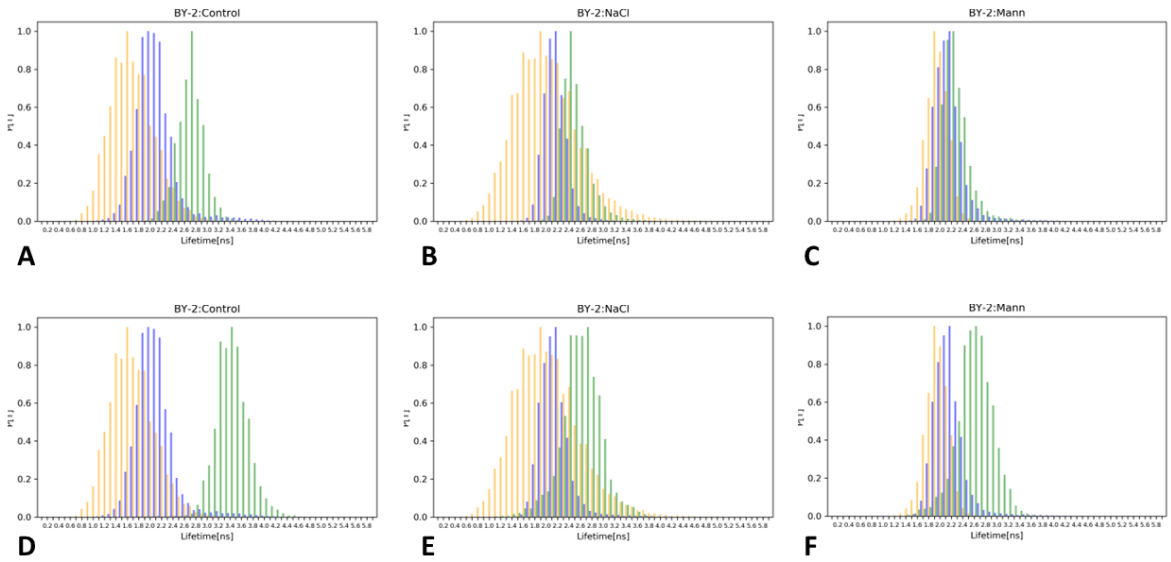

Fig. 3. Normalised distributions of the PEG-BDP lifetime derived from the cytoplasm of the BY-2 lines. Cytoplasmic signal (blue) is plotted together with the medium signal (orange) derived from cell vicinities and with stressed cells the cytoplasmic signal (green). (A-C) 200 mM NaCl stress; (D-F) 450 mM mannitol stress.

Then, BY-2 lines were analysed to determine how their cytoplasmic MC change in response to salt and mannitol stress. Increasing NaCl concentration (+200 mM) led to moderate level plasmolysis within an hour of all BY-2 lines. Such salt stress resulted in significantly altered PEG-BDP lifetime distributions in BY-2:Control in a timeline below 30 min (Table 1; Fig. 3A-C; Fig. 4). Both lifetime signals distributions and lifetime mean values went higher. This corresponds to an increase in MC in response to increased media osmolarity, that forces water efflux from the cells. Similar trends, but more prominent, were observed after an application of 450 mM mannitol to BY-2 media (Table 1). Moreover, adding extra mannitol led to severe plasmolysis within all lines, so massive water leakage from cells also occurred, which rapidly boosted MC. In both adapted lines increase in relative lifetime (Δ), as well as absolute mean lifetime increments were at least twice much smaller in adapted lines, than in BY-

2:Control (Table 1). Thus, we concluded, that changes in MC after stresses were the greatest in BY-2:Control, which lived in media of the lowest osmolarity and viscosity. Respectively, the changes were the smallest after stresses in BY-2:Mann, which live the media of the highest osmolarity (Fig. 3;Table 1). BY-2:NaCl and BY-2:Mann experienced relatively smaller hyperosmolarity stress when 200 mM NaCl or 450 mM mannitol were added. As a result of long-term osmoadaptation, BY-2 lines had obtained enduringly altered properties of the cytoplasm, which shape also their responses to hyperosmolarity.

	Mu - cytoplasm [ns]	Mu – medium [ns]	Delta[%] cytoplasm vs. medium	+200 mM NaCl; cytoplasm [ns]	Δmu NaCl stress vs nontreated cells [ns]	Δ[%] NaCl stress; cytoplasm vs. medium	+450 mM mannitol; cytoplasm [ns]	Δmu Mannitol stress vs nontreated cells [ns]	Δ[%] mannitol stress; cytoplasm vs. medium
BY-2:C	2.10 ± 0.13	1.69 ± 0.15	**24%**	2.67 ± 0.06	0.57	**58%**	3.40 ± 0.09	1.3	**101%**
BY-2:NaCl	2.18 ± 0.04	2.01 ± 0.33	**12%**	2.48 ± 0.07	0.3	**23%**	2.59 ± 0.12	0.41	**29%**
BY-2:Mann	2.17 ± 0.08	1.81 ± 0.04	**20%**	2.24 ± 0.07	0.07	**24%**	2.58 ± 0.10	0.41	**43%**

Table 1. Mean values (Mu) and standard deviation (±) values of lifetime PEG-BDP values derived from cytoplasm of BY-2 cells and medium in cells vicinity. The difference between cells and media was calculated and presented as Delta[%].

Interestingly, media from the vicinity of NaCl stressed cells presented much broader lifetime signal distributions than in the case of adapted cell media, despite similar compositions (Fig. 4). We suppose that it might be due to the releasing of cell walls components, like arabinogalactans, and disturbed endocytosis/exocytosis balance in response to increased NaCl concentrations (Lamport et al., 2006; Olmos et al., 2017; Zwiewka et al., 2015). However, such effect was not specific to NaCl stress and was observed also in BY-2:Control during mannitol stress, but not in adapted lines (Fig. 4). Surprisingly, after salt stress, BY-2:Mann and BY-2:NaCl distributions of lifetime signals in the cytoplasm differently surrounding media lifetime signals (Fig. 4). It also suggests that adapted BY-2 cells could be more resilient to water efflux induced by hyperosmolarity. For calculation of relative to medium lifetime (Δ) in stressed cells, the default line's medium signal was utilized, as equivalent of the reference and default cells environment (Table 1).

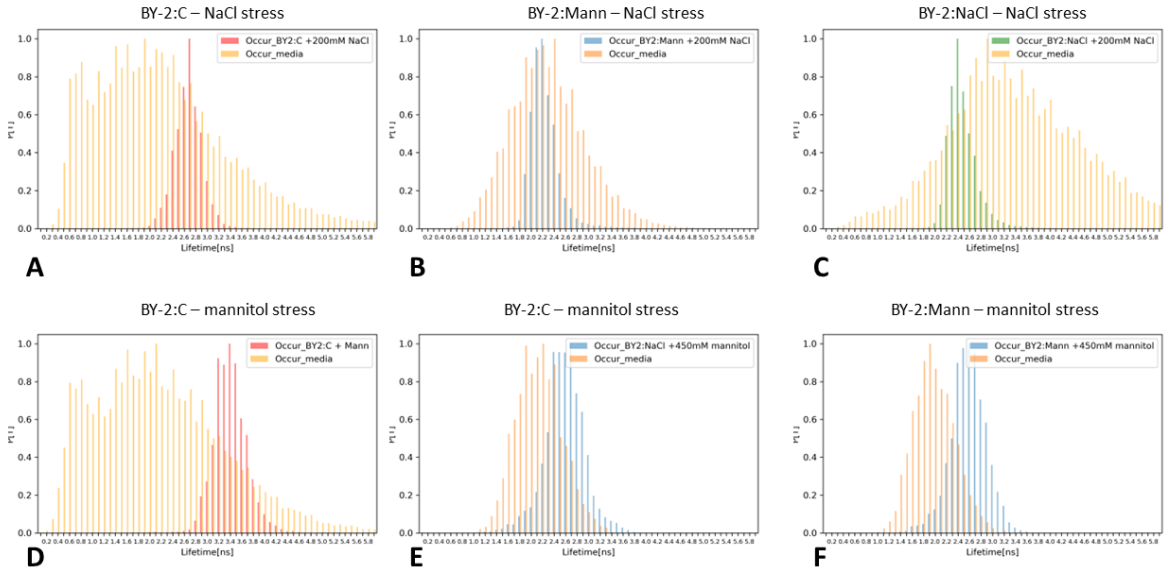

Fig. 4. Normalised lifetime distributions of the PEG-BDP signal derived from the cytoplasm of BY-2 lines that were subjected to 200 mM NaCl stress (A-C) and 450 mM mannitol stress (D-F). The cytoplasmic PEG-BDP lifetime signals distributions are plotted on the background of the media signal derived from the vicinity of the cells (orange).

Changes in MC over time after increasing NaCl concentrations were also studied by repeating the PEG-BDP lifetime imaging of the same population of BY-2:Control cells (SI_BDPimage.pdf). Lifetime distributions were floating toward higher values persistently through an hour and also became wider (Fig. 5). The increasing lifetime values showed a dynamic process of osmoadaptation, where a more viscous cytoplasm of BY-2:NaCl is an example of long-term NaCl-adapted cells. However, here during salt stress, MC got higher because of progressive cells plasmolysis. When significantly NaCl concentration is increase, cells could more or less gradually lose their ability to counterbalance and stop water efflux. In timescale of a day BY-2:Control cells die when cultured in medium enriched in 200 mM NaCl. Transitions of MC state induced by severe salt-induced hyperosmolarity seems not to be finished within an hour within a small population of cells. Does it correspond to advance in cells' deterioration, it's not clear yet.

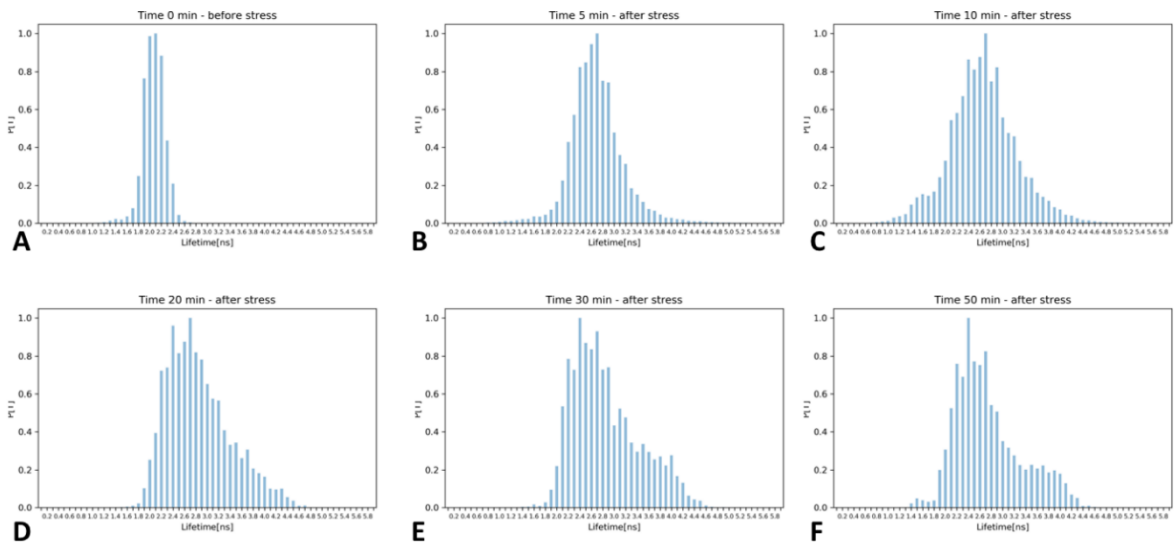

Fig. 5. Distributions of PEG-BDP lifetime signals from the same BY-2:Control population after increasing salinity (+200 mM NaCl). A – before adding media with NaCl; B-F) respectively 5, 10, 20, 30, 50 minutes after increasing the concentration of NaCl in the medium (salt stress).

'Rehydration' experiments were performed by removing after 15 min. 200 mM NaCl stress, the stress medium and then adding the default line medium. After next 15 minutes of cells 'recovery' and 'rehydartion', the cytoplasmic PEG-BDP lifetime distribution was measured. Revealed lifetime was intermediate level, between nontreated and NaCl stressed cells (Fig. 46). This result show, that 'recovery' of cellular microenvironment after hyperosmolarity stress takes also several minutes, but starts immediately. Hence, during 'rehydration', the similar dynamics to hyperosmolarity induced changes in MC was observed. Interestingly, the 'rehydration' media derived lifetime values exhibited much narrower distributions, than in the case of stress media.

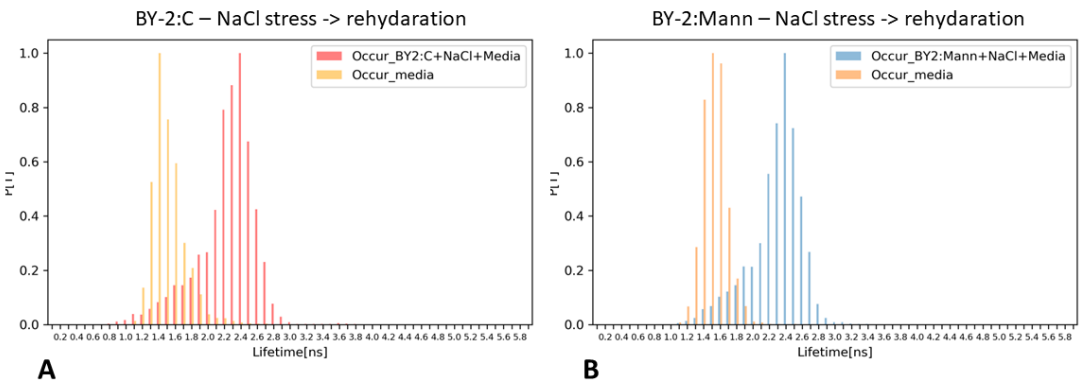

Fig. 6. Normalised lifetime distributions of the PEG-BDP signal derived from the cytoplasm of BY-2 cells that were subjected to 200 mM NaCl stress and then 'rehydration' with default media after 15 min. of NaCl stress. The cytoplasmic PEG-BDP lifetime signals distributions are plotted on the background of the media signal derived from the vicinity of the cells (orange). A) BY-2:NaCl; B) BY-2:Mann

The BY-2 lines were cultured under very different conditions, with very varied osmolarity. We revealed that suspension tobacco cells does not seem to preserve the same level of cytoplasmic molecular crowd after adaptation to high NaCl/mannitol. The another significant differences observed between the BY-2 lines were MC transitions after NaCl/mannitol stress. Although in all BY-2 lines the cytoplasmic PEG-BDP lifetime values became higher, in the adapted BY-2 lines the relative changes were smaller. The preservation of the cytoplasmic microenvironment within some range is required for

cell survival, but in severely altered osmotic conditions, the cytoplasm did not restore the properties observed in the reference conditions, even on a timescale of multiple generations. Furthermore, the cytoplasmic microenvironment of BY-2:NaCl and BY-2:Mann appears to make them less prone to stress-induced cytoplasm condensing.

Plasma membrane tension is lower in BY-2:NaCl, as well as in NaCl stressed cells

N^+-BDP rotors were shown to be an efficient tool for determining changes in plasma membrane tension (PM) (Michels et al., 2020). In BY-2 heterogeneity of the lifetime within PM and intracellular membranes was observed (Fig. 7). Importantly, the N^+-BDP lifetime derived from the medium decreased in high mannitol and high NaCl media. This showed that N^+-BDP exhibits different behaviour in hydrophilic liquid media and in semifluid lipid membranes (Table 2). Simultaneous interpretation of the lifetime of N^+-BDP derived from the medium (liquid) and the membranes to obtain relative to the 'delta' lifetime of the medium did not seem to be straightforward, so direct comparison of the lifetime values of PM was found to be more informative.

The mean value of N^+-BDP lifetime in PM of BY-2:Control was 4.16 ns. The PM lifetime distribution and the lifetime mean value (4.21 ns) were slightly higher in BY-2:NaCl than in BY-2:Control. Surprisingly, BY-2:Mann exhibited a significantly lower lifetime values distribution (mean: 3.82 ns), than PM in BY-2:Control (Table 2; Fig. 8; SI_BDPimage.pdf). This would suggest an increase in the PM tension in the PM of BY-2:Mann. Also, osmotic stress invoked by 450 mM mannitol had an surprising effect on the lifetime values of PM N^+-BDP, which declined. This would indicate greater PM fluidity and increased tension, as it would be expected in hypoosmolarity, but not hyperosmolarity. BY-2:Control stressed with 450 mM mannitol, as well as BY-2:Mann, were characterised by PM N^+-BDP lifetime distributions significantly lower than BY-2:Control (Table 2). It is counterintuitive: a longer lifetime and corresponding lower tension of the wrinkled plasma membrane were expected in the results of plasmolysis, which was observed in the case of BY-2:Control stressed with mannitol. Our results suggest that high concentrations of mannitol disturbed the lifetime of N^+-BDP and made such a sample incomparable to BY-2:Control. The plasmolyzed, mannitol stressed BY-2:Control exhibited much lower N^+-BDP lifetime in PM (3.50 ns), than non-plasmolyzed BY-2:Mann (3.82 ns) with the same mannitol concentration. It might be speculated that the approximate difference between these values (0.32 ns) was related to decreased PM tension, as an result of plasmolysis of mannitol stressed cells.

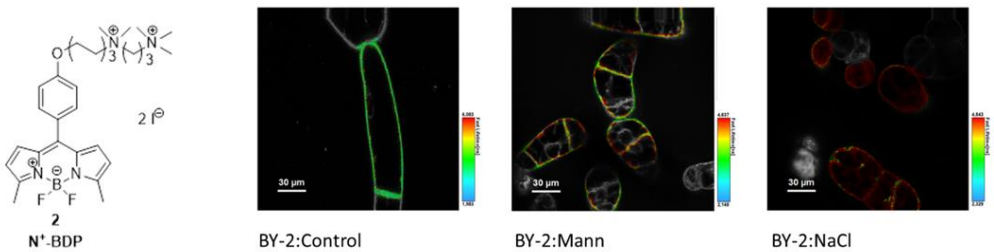

Fig. 7. N^+-BDP formula and N^+-BDP stained BY-2 lines. The images are on false colour scale, representing the mean fluorescence lifetime for each pixel, expressed in nanoseconds.

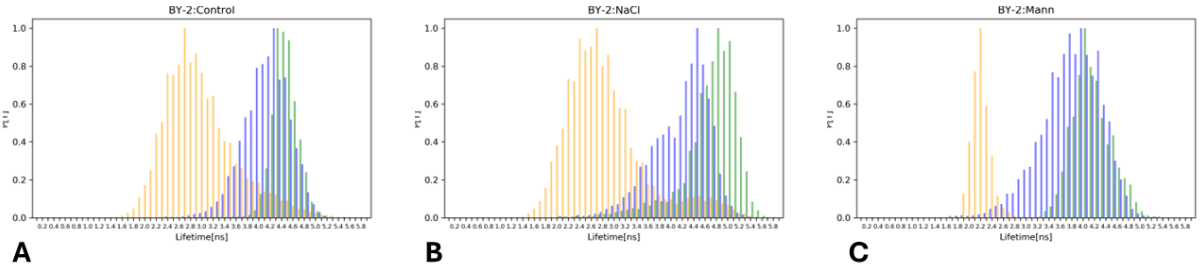

Fig. 8. Normalised lifetime distributions of the N⁺-BDP signal derived from the plasma membrane of BY-2 lines (blue), which were subjected to additional NaCl stress (green). The plasma membrane signal is plotted on the background of the media signal derived from the vicinity of the cells (orange).

	Mu – plasma membrane [ns]	Mu – media [ns]	Δmu PM vs media [ns]	+200 mM NaCl [ns]	Δmu NaCl stress vs. nontreated cells [ns]	Δmu Mann stress vs nontreated cells [ns]	Δmu mann. stress vs. nontreated cells [ns]
BY-2:C	4.16 ± 0.16	2.98 ± 0.41	1.18	4.42 ± 0.56	0.26	3.50 ± 0.20	-1.16
BY-2:NaCl	4.21 ± 0.25	2.85 ± 0.03	1.36	4.65 ± 0.25	0.44	3.98 ± 0.17	-4.23
BY-2:Mann	3.82 ± 0.27	2.21 ± 0.50	1.61	4.11 ± 0.12	0.29	n/a	n/a

Table 2. Mean values (Mu) and standard deviation (±) values of lifetime N⁺-BDP values derived from plasma membrane of BY-2 cells and medium in cells vicinity.

N^+-BDP lifetime in plasma membranes of BY-2:Control cells after 200 mM NaCl stress exhibited the distribution shifted toward higher values. The mean lifetime value also increased by 0.26 ns. This implicates decreased PM tension that occurred in response to hyperosmolarity, that correspond to observed moderate plasmolysis level. N^+-BDP lifetime exhibited higher values also in the PM of BY-2:NaCl and BY-2:Mann in response to 200 mM NaCl stress (Table 2; Fig. 8). Interestingly, plasma membranes of cells subjected to salt stress seem to have the most altered N^+-BDP signals in BY-2:NaCl; with mean value increased of 0.44 ns. It suggests that PM tension changed the most in salt stressed BY-2:NaCl. The moderate plasmolysis was observed within an hour in all three lines after increasing NaCl concentration in media. The base level of the N^+-BDP lifetime is also the highest in BY-2:NaCl, so it suggest that long term culturing of BY-2 in high NaCl might not made them more resilient to increased salinity.

Our results suggest that through the adaptation process PM tension in BY-2:NaCl decreased. Such feature might be related to altered BY-2:NaCl morphology and smaller cells size. Also NaCl stress reduced PM tension in both BY-2:Control and the adapted ones, what correlate with plasmolysis. Additionally, obtaining PM properties was found not to be feasible in the case of media that have substantial different mannitol concentrations.

Brillouin spectrum values revealed differences in viscoelasticity between BY-2:Control and adapted lines

The distributions of the Brillouin line shift, $f_{B,medium}$, and linewidth, $g_{B,medium}$, for pure BY-2 media are presented in Fig. 9. The distributions of the media are narrow. Brillouin line shift and the linewidth for each medium are significantly higher than those observed in bulk water. The lowest values of both Brillouin measurable are found for BY-2:Control medium, a bit higher values correspond to BY-2:NaCl medium and the highest were found for BY-2:Mann medium. This result reflects the gradual increase in concentration and type of solutes in prepared culture media (BY-2:Control-> BY-2:NaCl-> BY-2:Mann).

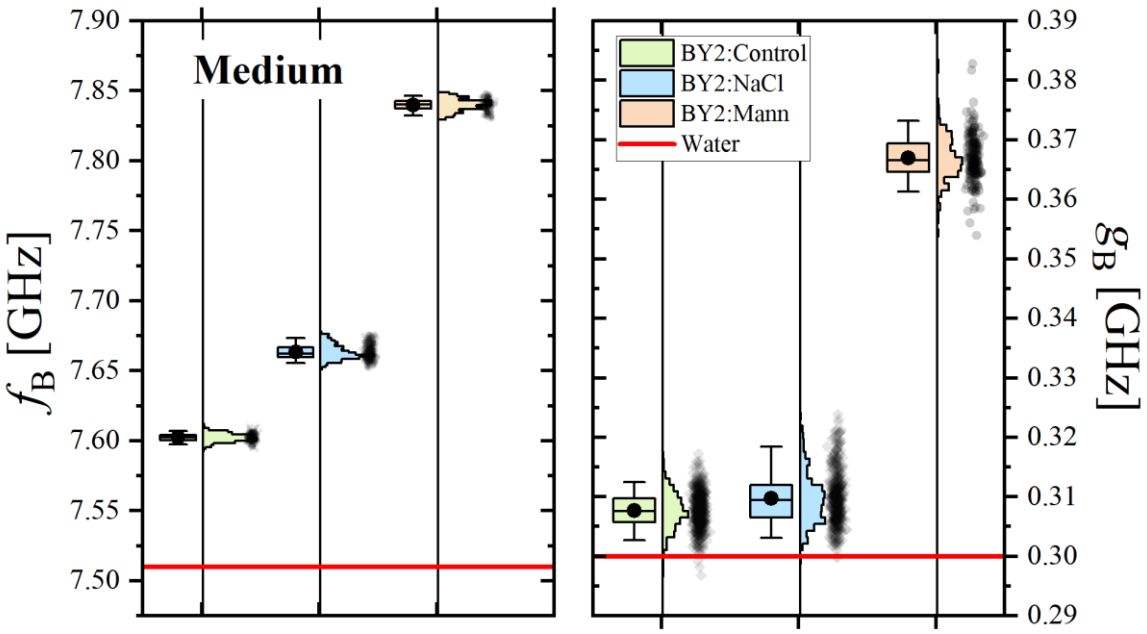

Fig. 9. Distributions of Brillouin line shift, fB, and linewidth, gB, for pure media. Horizontal red lines indicate values for bulk water.

Distributions of Brillouin line shift and line width for vacuole and cytoplasm dominating areas (Fig. 1e) are presented on Fig. 10 and Fig. 11. The distributions of those values are much broader (than those for pure media) being the joint result of inhomogeneity of cells and variations in cells properties. The values of both Brillouin parameters are distinctly higher than those found in pure media buffers. This is the manifestation of a trivial fact that cells are much more concentrated than liquid media. Significantly, if the cell lives in a buffer characterised by higher Brillouin line-shift (or linewidth), its protoplast is also characterised by higher Brillouin measurable. The cells become more crowded, if it is exposed to a more concentrated environment of higher osmolarity. In result: 1) water is relatively more excreted from the cell, or 2) cells produce more molecules to increase molecular crowd. However, it is hard to say which of the above two has the highest contribution, since Brillouin is measurable depending on quantity (concentration) and quality (specific compounds dissolved) (Adichtchev et al., 2019; Yan et al., 2021).

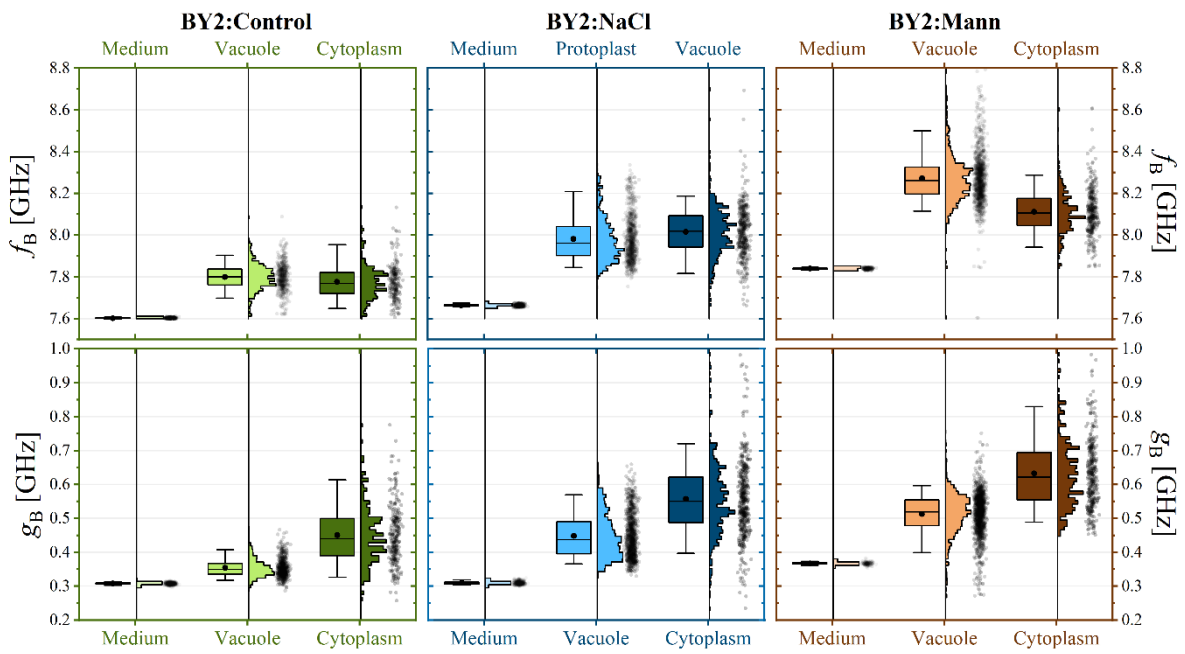

Fig. 10. Distributions of the Brillouin line shift, f_B,(upper panels) and Brillouin line width, g_B, (lower panels) for pure media, cell vacuoles and cytoplasm for three cell lines of cells (BY-2:Control – green, BY-2:NaCl – blue, BY-2:Mann – brown).

To better visualise the effect of medium on cell mechanical properties, Brillouin results were presented in the form of the relative Brillouin shift (named 'elastic contrast' in (Bacete et al., 2021)), υ_B, and the relative Brillouin line width ("viscous-like contrast"), γ_B, according to

$$\begin{aligned} \upsilon_B &= f_B \,/\, f_{B,buffer} - 1 \\ \gamma_B &= g_B \,/\, g_{B,buffer} - 1 \end{aligned} \quad \text{(x7)}$$

It should be emphasised that the definitions of mechanical contrasts (elastic and viscous) adopted in this study differ from the usual ones (Antonacci et al., 2020), where changes in Brillouin line shape parameters are given in relation to the values characterising pure bulk water. We decided to express the contrasts relative to the media, as these are the natural environments of the examined cells. Nonzero values of such defined mechanical contrasts can be interpreted in terms of change of internal composition being the result of cells adaptation.

The distributions of elastic and viscous contrasts are presented in Fig. 11.

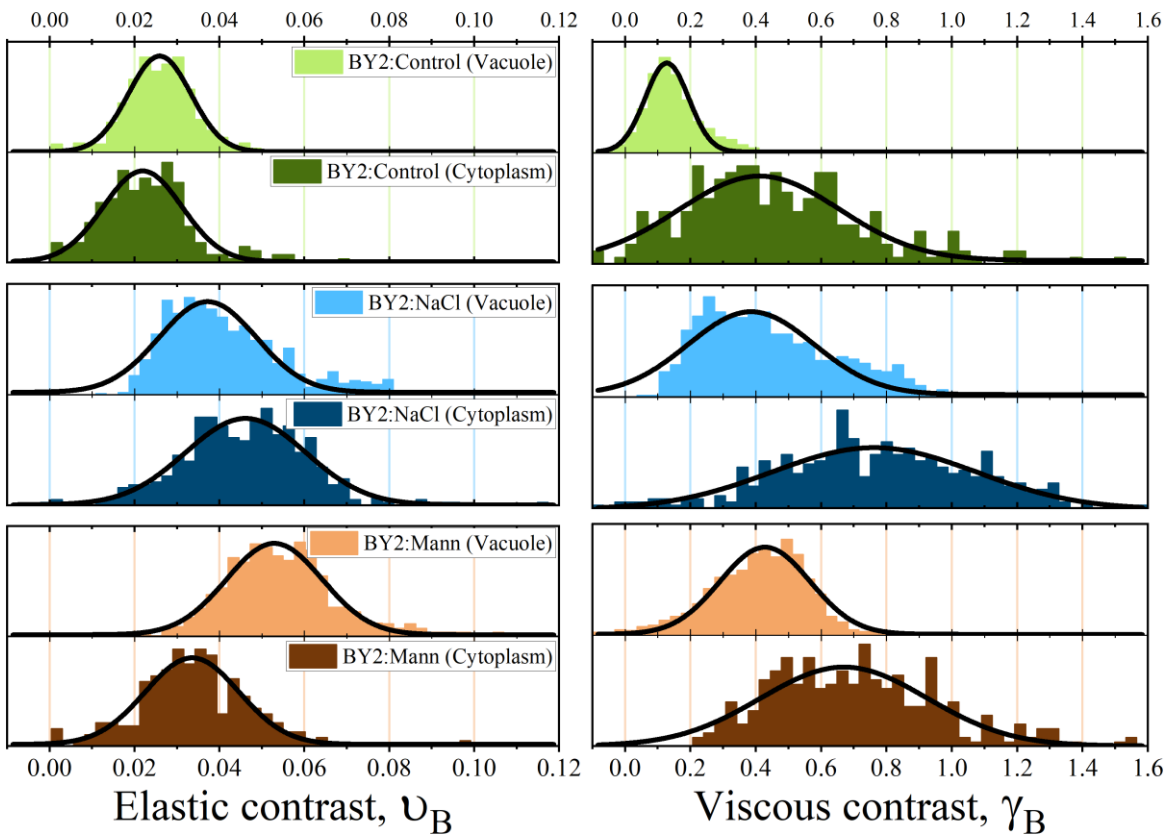

Fig. 11. Distributions of relative Brillouin shift fB, and relative Brillouin line width, gB, for vacuoles dominating areas and cytoplasm dominating areas for three cell lines of cells (BY-2:Control – green, BY-2:NaCl – blue, BY-2:Mann – brown).

The BY-2 cell lines exhibit different Brillouin values υ_B and γ_B. Few interesting observations can be made from the data presented in Fig. 9, Fig. 10, Fig. 11, and Table 3:

1) The distributions of elastic and viscous contrasts for the vacuoles are the narrowest for BY-2:Control cells, suggesting that these are the most homogeneous cells on both the population scales and the single cell scales.
2) The relative Brillouin shift (elastic contrast) found for the vacuoles of the BY-2:Control cells is about 2.5% higher than its medium. For BY-2:NaCl cells it is about 4% higher, whereas for cells living in high mannitol, BY-2:Mann, the mean value is 5%. If we recall that the Brillouin shift depends on the compressibility of the system (which changes with molecules concentration), and if we accept that vacuoles can be treated as an aqueous mixture, then we can interpret this result as an indication of molecular crowding. The effect is specific for a given culture medium, which is the highest for BY-2:Mann, followed by BY-2:NaCl, and the lowest for BY-2:Control.
3) A qualitatively similar trend is observed for the viscous contrast (relative Brillouin width) obtained for the vacuoles. Here, the mean values of the distributions starting from 13% for BY-2:Control cells, followed by 39% for BY-2:NaCl cells. The highest values of 43% are again observed for BY-2:Mann.
4) The above analysis of the distributions of elastic and viscous contrasts suggests that long-term exposure of cells to concentrated both NaCl and mannitol makes the vacuoles more crowded and viscous. This effect in BY-2:Mann is more pronounced. The result of crowding is the reduction of the compressibility of the mixture and the increase in longitudinal viscosity. Brillouin values revealed variability in viscoelastic properties between cells adapted to various osmotic conditions.

5) Different results appeared when comparing the mechanical contrasts (both, elastic and viscous) recorded in cytoplasmic areas. Here, the highest values were found for BY-2:NaCl.
6) Interestingly, only for BY-2:NaCl, the elastic contrast of cytoplasm is higher than the vacuole. Exposition to other media makes the vacuoles more compressible. Vacuole in BY-2:NaCl is involved in both osmoregulation, as well as for Na^+ sequestration. In BY-2:NaCl NaCl is in the medium in the highest concentration, what impose extra threat to cells, despite high osmolarity.
7) On the other hand, the elastic contrast values of vacuole are greater, than the elastic contrast values of cytoplasm, in the highest rate in BY-2:Mann. This might be consequences of the highest osmolarity to which are exposed BY-2:Mann, what led to the prominent alteration in cellular and media water activity. Significantly, also the highest absolute elastic and viscous BLS values were observed in BY-2:Mann.

Interestingly, BLS results show that exposure to different culture media not only changed the overall composition of the cell, but also induced spatial inhomogeneity of this composition. This is partially confirmed by the observation that cells exposed to NaCl showed the broadest and clearly asymmetric distributions of mechanical contrasts (elastic and viscous) being skewed toward higher values.

	υ_B [%] (Elastic contrast)		γ_B [%] (Viscous contrast)	
	Vacuole	Cytoplasm	Vacuole	Cytoplasm
BY-2:Control	2.59 ± 0.37	2.19 ± 0.93	12.79 ± 6.67	41.15 ± 24.55
BY-2:NaCl	3.72 ± 1.15	4.62 ± 1.42	38.59 ± 19.31	76.19 ± 31.34
BY-2:Mann	5.29 ± 1.13	3.36 ± 1.11	42.83 ± 13.83	67.00 ± 25.53

Table 3. Elastic (υ_B) and viscous (γ_B) contrast values measured for different regions of the cells (cytoplasm and vacuole) belonging to three different lines. The values were obtained as a mean of the distribution (presented in Fig. 11 whereas the uncertainty (±) is the standard deviation.

BLS allows for tracking dynamic elastic contrast changes in BY-2 during salt stress

BY-2:Control cells were exposed to their media enriched in additional 200 mM NaCl. The samples were immediately transferred under the microscope and, after the beam was focused in the desired position within a cell, the Brillouin spectra were acquired in time (Fig. 12). The acquisition time of a single spectrum was ~10 s. The relative Brillouin shifts obtained increase in time for NaCl stress. The increase in Brillouin shift is expected in hyperosmotic stress as water efflux from cells occur. Here, we observed - on the single cell scale, increase in the Brillouin shift and its stabilisation after approx. 12 min. Similar time traces for spheroids were recently presented (Bevilacqua et al., 2023; Zhang et al., 2023). Here, we showed that BLS might be utilized also in time resolved analysis of cells properties.

Further development, including shortening the time required for data acquisition or improving spatial resolution, would make BLS a more powerful tool in revealing cell responses to fluctuating environmental factors (Bevilacqua et al., 2023; Zhang et al., 2023).

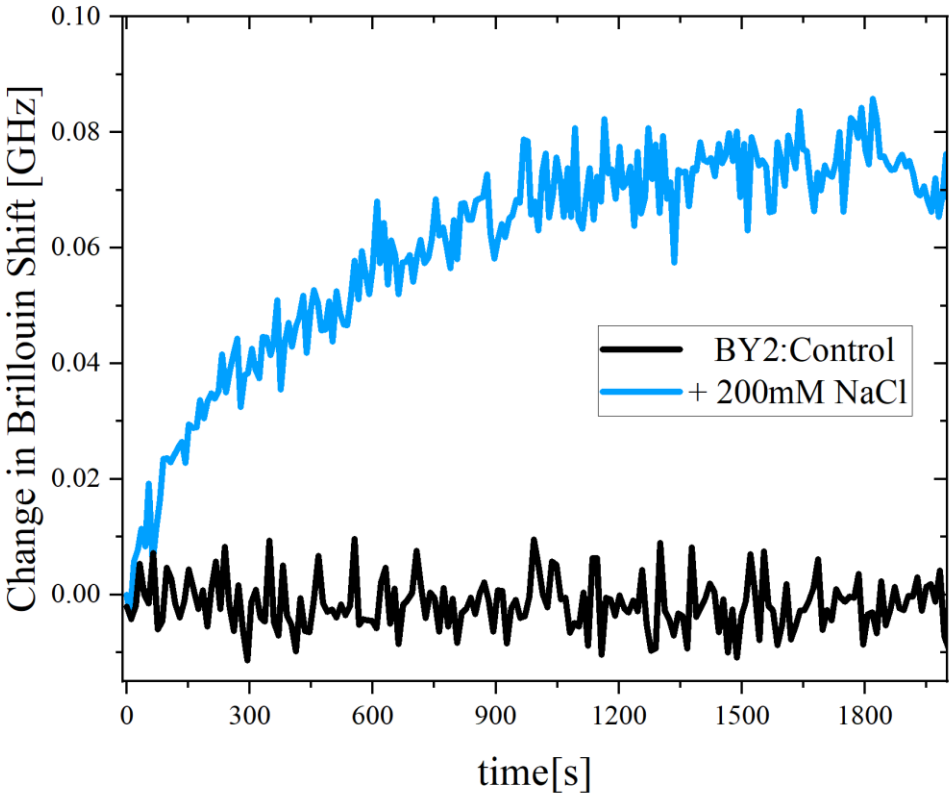

Fig. 12. Representative change in time of the Brillouin shift (relative to the value at time=0) after osmotic shock with medium enriched in 200 mm NaCl. Spectra were analysed with a single phase model (eq.x5). The change in Brillouin shift is presented (BY-2:Control + 200 mM NaCl – blue; BY-2: Control without treatment - black). The time from cell exposition to starting measurement time 0 s was less than 2 min.

Discussion

Understanding the interrelations between a cellular microenvironment and an external environment remains a significant challenge in plants cell biology. One fundamental environmental factor with pleiotropic impact is osmolarity, which can rapidly alter water activity and directly affect all cellular processes and biomechanical balance within plants cells elements (Watson et al., 2023; Zonia & Munnik, 2007). Plant cells sense the mechanical signals at the cell wall, plasma membrane and inside the cell. Information from these different cellular compartments is integrated to develop adaptive responses and maintain mechanical homeostasis at the cellular level (Cosgrove, 1993; Geitmann & Ortega, 2009). Although the significance of cell and tissue mechanics in plant development has been appreciated for many years (Echevin et al., 2019; Moulia et al., 2015, 2019, 2021; Trinh et al., 2021), the study of cellular micromechanics at the level of the individual cell has proven to be problematic. The universal presence of the cellulosic cell wall and the apoplastic continuity that it provides endows plant tissues with a unique level of mechanical coupling. In principle, this makes it possible for plant tissues to transmit stress-mechanical information precisely and instantaneously over multicellular distances. However, the same apoplastic continuity that makes stress-mechanical signaling attractive as a possible developmental effector also makes it difficult to interpret responses and isolate mechanical variables at the level of the individual cell. Using individual cells cultivated in suspension helps control these variables, making it easier to interpret how cells respond to a given environmental stimulus. Such model system allows to study plant biomechanical properties and their regulation by

various extrinsic and intrinsic factors influenced by the physical interactions between cells and their environment (Weber et al., 2015).

In our research, we investigated the viscoelastic properties of plant cells adapted to severe osmotic conditions and, subsequently, their properties changes in response to stress. We utilised cells exposed to high concentrations of NaCl or mannitol in the short-term ('stress') or long-term conditions ('adaptation') to establish a useful model to elucidate cellular responses to hyperosmolarity. A morphological and cell aggregation aberrances of BY-2:NaCl show that osmoadaptation does not necessarily result in reestablishing cell biology of reference cells. In contrast to BY-2:NaCl, the BY-2:Mann morphology and growth more resembles the BY-2:Control . In *S. cerevisiae* it was shown, that starvation leads to decreased cells size and increased molecular crowd (Joyner et al., 2016). There is not enough data yet to correlate small size and crowdedness of BY-2:NaCl cells with 'starvation-like' effect. However, high osmolarity of BY-2:Mann medium did not lead to the decreased cells size, so this effect might be salinity dependent disturbance of cells metabolism regulation or effectiveness.

The adapted BY-2 lines are characterized also by very different abiotic stress related gene expression patterns (Skrzypczak et al., 2024). Both adapted cell lines successfully mitigated the prolonged risk of increased molecular crowding, membrane disintegration, and other disruptions triggered by hyperosmolarity stress. It is important to note that the impacts of NaCl on cells go beyond hyperosmolarity, and includes sodium-specific toxicity and increased ionic strength, which can disturb the cellular microenvironment (Honig & Nicholls, 1995). However, at some rate mannitol also increases ionic strength by inducing water efflux from cells, followed by a regulatory volume increase through the uptake of ions and relative increase in ionic cellular constituents (Zonia & Munnik, 2007). In future, advances in cellular biosensors of ionic strength could help to distinguish effects of ionic strength and osmolarity/water activity on cells (Liu et al., 2017; Miller et al., 2020).

Recent studies have demonstrated that in neuroblastoma cells hyperosmolarity rapidly increases cellular viscosity and molecular crowding (Kitamura et al., 2023). In human cell lines, the conservation of viscosity across numerous cell lines indicates the importance of maintaining viscosity within a certain range (Kwapiszewska et al., 2020). However, this may not be the case in plant cells, where physical forces are different and largely determined by cell walls and turgor pressure. The altered viscoelasticity observed in long-term BY-2 cultures adapted to high NaCl/mannitol concentrations highlights the potential of plant cells to function with persistently altered viscoelastic properties.

The PEG-BDP rotors allowed us to discover a more crowded cytoplasm in BY-2 cells adapted to high NaCl/mannitol, with smaller differences between molecular crowding in cellular and media in BY-2:Mann/NaCl compared to BY-2:Control. The increased MC is related to lower water activity and higher osmolarity and would have a pleiotropic impact on molecular processes in cells. More crowded cytoplasm might be the result of adaptive synthesis of osmolytes, composition of ions, and the population of Intrinsically Disordered Proteins (IDP). However, BLS revealed that the relative differences between the environment in the media and the cytoplasm dominating areas were greater in adapted cells than in BY-2:Control. Such difference requires further research to point out does it depend on various measured phenomenon or not. Relations between osmolarity, water activity, MC, viscosity, and ionic strength in cellular microenvironments are close, but also complex, and challenging to elucidate *in situ*.

In recent years, Intrinsically Disordered Proteins (IDPs) have emerged as key players in stress response and plant development (Hsiao, 2022; Hsiao et al., 2020; Zamora-Briseño et al., 2021). After hyperosmolarity or heat stress, a new homeostatic set point is rapidly obtained by establishing an appropriate set of IDP in fibroblasts (Watson et al., 2023). Late Embryogenesis Abundant (LEA) proteins, the most prevalent IDPs in plants, are involved in stress response and tolerance (Hernández-Sánchez et al., 2022; Romero-Perez et al., 2023). *The N. tabacum* LEA genes have been identified and shown to

respond to ABA and NaCl in a selective manner (Geng et al., 2022). However, none of them, i.e. 123 identified *N. tabacum* LEA genes, was significantly up- or down-regulated in adapted BY-2 lines in our RNA-seq differential gene analysis (Skrzypczak et al., 2024).

Vacuoles play a crucial role in plant cell osmoregulation, and their content and mechanical properties are important for the response to cellular stress (Afzal et al., 2016; Maurel et al., 1997). How could works coordination between PM and tonoplast ions and water transport has been proposed for guard cells (Cubero-Font & De Angeli, 2021). By BLS we obtained data on approximate vacuoles areas, that were distinguished from cytoplasmic bands areas pushed to cell walls by vacuole's pressure. We did not have the possibility to integrate BLS with fluorescence microscopy, which would have allowed for a more precise identification of the subcellular compartment being measured. We revealed interesting properties of measured by BLS elastic contrast in BY-2:NaCl. Only in this one adapted line BLS measured molecular crowd seems to be higher in cytoplasm, than in vacuoles. It is tempting to speculate that intense sodium sequestration in BY-2:NaCl vacuoles impose deviation to vacuole/cytoplasm interface. In a tonoplast there are aquaporins and ion channels that would allow for regulation of cytoplasm/vacuole interface. MC is related to osmolarity and water activity, however in complex cellular environment these parameters are not easily distinguishable. Consequently, disturbance in vacuole's physiology and hypothetical low turgor, might have been significant factor in inducing disruption of BY-2:NaCl cells growth. However, still more specific research on relation of vacuoles to cytoplasm microenvironments are required to explain plants osmoadaptation.

Many questions remain to be answered regarding hyperosmolarity adaptation mechanisms. For instance, how do adapted BY-2 cells maintain efficient molecular machinery despite increased molecular crowd? Is the osmosensing machinery persistently hyperactivated in adapted BY-2 cells? Although osmoregulation mechanisms in plants have yet to be fully elucidated, mechanosensitive channels likely play a crucial role in osmosensing (Gorgues et al., 2022; Mousavi et al., 2021). In animal cells, the detection of osmotic stress is associated with the activity of kinase ASK3 (MAP3K16), which depends on the location within poly(ADP-ribose) containing condensates, coupled with liquid-liquid phase separation and cascades of the signalling pathway (Naguro et al., 2012; Watanabe et al., 2021). In plants, mono- and poly(ADP-ribosyl)ation was shown as involved in immunity, that often exhibits crosstalk with abiotic stress response (Feng et al., 2015; Kong et al., 2021; Yao et al., 2021). Importantly, viscoelasticity has been indicated as an important factor in liquid-liquid phase separation processes in biological systems (Tanaka, 2022).

Our work also demonstrates the utility of BLS in investigating viscoelasticity in plant cells cultured under various osmotic conditions. To our knowledge, this is the first time BLS has been utilised for the analysis of molecular crowding and viscosity in plant cells. Further expansion of Brillouin spectroscopy could provide beneficial data in studying plant cell responses to osmotic stress. Adding improved z-axis resolution and accelerating scanning would pave the way for cellular resolution when scanning multicellular organs like roots. As shown, correlating Brillouin spectroscopy with fluorescence microscopy would allow for correlating mechanical properties mapping with various subcellular structures. We suppose that BLS could become a very valuable tool for revealing cell reactions that involve alterations of the cellular microenvironment.

Author contributions

P.W., A.K-M., and T.S. conceptualized the study. T.S. and M.P. performed the experiments with BY-2 cells and analyzed the data. M.R. synthesized BDP-molecular rotors. T.S. and M.P. wrote the original draft, and A.K-M. reviewed the manuscript.

Funding

The work was supported by Polish National Science Centre (2020/39/B/NZ9/03336; to AKM), by School of Sciences, Adam Mickiewicz University (Interdisciplinary research grant BNSNS023; to MR, MP, TS), by Inicjatywa Doskonałości - Uczelnia Badawcza (038/04/NP/0025 to AKM).

References

Adichtchev, S. V., Karpegina, Yu. A., Okotrub, K. A., Surovtseva, M. A., Zykova, V. A., & Surovtsev, N. V. (2019). Brillouin spectroscopy of biorelevant fluids in relation to viscosity and solute concentration. *Physical Review E*, *99*(6), 062410. https://doi.org/10.1103/PhysRevE.99.062410

Afzal, Z., Howton, T. C., Sun, Y., & Mukhtar, M. S. (2016). The roles of aquaporins in plant stress responses. In *Journal of Developmental Biology* (Vol. 4, Issue 1). MDPI Multidisciplinary Digital Publishing Institute. https://doi.org/10.3390/jdb4010009

Alfano, C., Fichou, Y., Huber, K., Weiss, M., Spruijt, E., Ebbinghaus, S., De Luca, G., Morando, M. A., Vetri, V., Temussi, P. A., & Pastore, A. (2023). Molecular Crowding: The History and Development of a Scientific Paradigm. In *Chemical Reviews*. American Chemical Society. https://doi.org/10.1021/acs.chemrev.3c00615

Antonacci, G., Beck, T., Bilenca, A., Czarske, J., Elsayad, K., Guck, J., Kim, K., Krug, B., Palombo, F., Prevedel, R., Scarcelli, G., & Prevedel prevedel, R. (2020). *Recent progress and current opinions in Brillouin microscopy for life science applications*. https://doi.org/10.1007/s12551-020-00701-9/Published

Antonacci, G., Foreman, M. R., Paterson, C., & Török, P. (2013). Spectral broadening in Brillouin imaging. *Applied Physics Letters*, *103*(22), 221105. https://doi.org/10.1063/1.4836477

Bacete, L., Schulz, J., Engelsdorf, T., Bartosova, Z., Vaahtera, L., Yan, G., Gerhold, J. M., Tich, T., Øvstebø, C., Gigli-Bisceglia, N., Johannessen-Starheim, S., Margueritat, J., Kollist, H., Dehoux, T., Mcadam, S. A. M., & Hamann, T. (2021). *THESEUS1 modulates cell wall stiffness and abscisic acid production in Arabidopsis thaliana*. https://doi.org/10.1073/pnas.2119258119/-/DCSupplemental

Bevilacqua, C., Gomez, J. M., Fiuza, U. M., Chan, C. J., Wang, L., Hambura, S., Eguren, M., Ellenberg, J., Diz-Muñoz, A., Leptin, M., & Prevedel, R. (2023). High-resolution line-scan Brillouin microscopy for live imaging of mechanical properties during embryo development. *Nature Methods*, *20*(5), 755–760. https://doi.org/10.1038/s41592-023-01822-1

Colin, L., Martin-Arevalillo, R., Bovio, S., Bauer, A., Vernoux, T., Caillaud, M.-C., Landrein, B., & Jaillais, Y. (2022). Imaging the living plant cell: From probes to quantification. *The Plant Cell*, *34*(1), 247–272. https://doi.org/10.1093/plcell/koab237

COSGROVE, D. J. (1993). Wall extensibility: its nature, measurement and relationship to plant cell growth. *New Phytologist*, *124*(1), 1–23. https://doi.org/10.1111/j.1469-8137.1993.tb03795.x

Cubero-Font, P., & De Angeli, A. (2021). Connecting vacuolar and plasma membrane transport networks. In *New Phytologist* (Vol. 229, Issue 2, pp. 755–762). Blackwell Publishing Ltd. https://doi.org/10.1111/nph.16983

Cuevas-Velazquez, C. L., Vellosillo, T., Guadalupe, K., Schmidt, H. B., Yu, F., Moses, D., Brophy, J. A. N., Cosio-Acosta, D., Das, A., Wang, L., Jones, A. M., Covarrubias, A. A., Sukenik, S., & Dinneny, J. R. (2021). Intrinsically disordered protein biosensor tracks the physical-chemical effects of osmotic stress on cells. *Nature Communications*, *12*(1). https://doi.org/10.1038/s41467-021-25736-8

Echevin, E., Le Gloanec, C., Skowrońska, N., Routier-Kierzkowska, A.-L., Burian, A., & Kierzkowski, D. (2019). Growth and biomechanics of shoot organs. *Journal of Experimental Botany*, *70*(14), 3573–3585. https://doi.org/10.1093/jxb/erz205

Elsayad, K., Werner, S., Gallemí, M., Kong, J., Guajardo, E. R. S., Zhang, L., Jaillais, Y., Greb, T., & Youssef Belkhadir, ¶. (2016). *Mapping the subcellular mechanical properties of live cells in tissues with fluorescence emission-Brillouin imaging*. https://doi.org/10.1126/scisignal.aaf6326

Farokh Payam, A., & Passian, A. (2024). Imaging beyond the surface region: Probing hidden materials via atomic force microscopy. *Science Advances*, *9*(26), eadg8292. https://doi.org/10.1126/sciadv.adg8292

Feng, B., Liu, C., de Oliveira, M. V. V, Intorne, A. C., Li, B., Babilonia, K., de Souza Filho, G. A., Shan, L., & He, P. (2015). Protein Poly(ADP-ribosyl)ation Regulates Arabidopsis Immune Gene Expression and Defense Responses. *PLOS Genetics*, *11*(1), e1004936-. https://doi.org/10.1371/journal.pgen.1004936

Flowers, T. J., & Colmer, T. D. (2015). Plant salt tolerance: Adaptations in halophytes. *Annals of Botany*, *115*(3), 327–331. https://doi.org/10.1093/aob/mcu267

Gavish, B., & Werber, M. M. (1979). Viscosity-dependent structural fluctuations in enzyme catalysis. *Biochemistry*, *18*(7), 1269–1275. https://doi.org/10.1021/bi00574a023

Geilfus, C. M. (2018). Chloride: From Nutrient to Toxicant. *Plant and Cell Physiology*, *59*(5), 877–886. https://doi.org/10.1093/pcp/pcy071

Geitmann, A., & Ortega, J. K. E. (2009). Mechanics and modeling of plant cell growth. *Trends in Plant Science*, *14*(9), 467–478. https://doi.org/10.1016/j.tplants.2009.07.006

Geng, W., Wang, Y., Zhang, J., Liu, Z., Chen, X., Qin, L., Yang, L., & Tang, H. (2022). Genome-wide identification and expression analyses of late embryogenesis abundant (LEA) gene family in tobacco (Nicotiana tabacum L.) reveal their function in abiotic stress responses. *Gene*, *836*. https://doi.org/10.1016/j.gene.2022.146665

Gorgues, L., Li, X., Maurel, C., Martinière, A., & Nacry, P. (2022). Root osmotic sensing from local perception to systemic responses. In *Stress Biology* (Vol. 2, Issue 1). Springer. https://doi.org/10.1007/s44154-022-00054-1

Gouveia, R. M., Lepert, G., Gupta, S., Mohan, R. R., Paterson, C., & Connon, C. J. (2019). Assessment of corneal substrate biomechanics and its effect on epithelial stem cell maintenance and differentiation. *Nature Communications*, *10*(1), 1496. https://doi.org/10.1038/s41467-019-09331-6

Hayot, C. M., Forouzesh, E., Goel, A., Avramova, Z., & Turner, J. A. (2012). Viscoelastic properties of cell walls of single living plant cells determined by dynamic nanoindentation. *Journal of Experimental Botany*, *63*(7), 2525–2540. https://doi.org/10.1093/jxb/err428

Hernández-Sánchez, I. E., Maruri-López, I., Martinez-Martinez, C., Janis, B., Jiménez-Bremont, J. F., Covarrubias, A. A., Menze, M. A., Graether, S. P., & Thalhammer, A. (2022). LEAfing through literature: late embryogenesis abundant proteins coming of age - achievements and perspectives. In *Journal of Experimental Botany* (Vol. 73, Issue 19, pp. 6525–6546). Oxford University Press. https://doi.org/10.1093/jxb/erac293

Honig, B., & Nicholls, A. (1995). Classical Electrostatics in Biology and Chemistry. *Science*, *268*(5214), 1144–1149. https://doi.org/10.1126/science.7761829

Hoque, M. A., Banu, M. N. A., Okuma, E., Amako, K., Nakamura, Y., Shimoishi, Y., & Murata, Y. (2007). Exogenous proline and glycinebetaine increase NaCl-induced ascorbate-glutathione cycle enzyme activities, and proline improves salt tolerance more than glycinebetaine in tobacco Bright Yellow-2 suspension-cultured cells. *Journal of Plant Physiology*, *164*(11), 1457–1468. https://doi.org/10.1016/j.jplph.2006.10.004

Hsiao, A. S. (2022). Plant Protein Disorder: Spatial Regulation, Broad Specificity, Switch of Signaling and Physiological Status. *Frontiers in Plant Science*, *13*. https://doi.org/10.3389/fpls.2022.904446

Hsiao, A. S., Wang, K., & Ho, T. H. D. (2020). An intrinsically disordered protein interacts with the cytoskeleton for adaptive root growth under stress. *Plant Physiology*, *183*(2), 570–587. https://doi.org/10.1104/pp.19.01372

Jelínková, A., Müller, K., Fílová-Parezová, M., & Petrášek, J. (2015). NtGNL1a ARF-GEF acts in endocytosis in tobacco cells. *BMC Plant Biology*, *15*(1), 1–14. https://doi.org/10.1186/s12870-015-0621-3

Joyner, R. P., Tang, J. H., Helenius, J., Dultz, E., Brune, C., Holt, L. J., Huet, S., Mü ller, D. J., & Weis, K. (2016). *A glucose-starvation response regulates the diffusion of macromolecules*. https://doi.org/10.7554/eLife.09376.001

Julkowska, M. M., & Testerink, C. (2015). Tuning plant signaling and growth to survive salt. *Trends in Plant Science*, *20*(9), 586–594. https://doi.org/10.1016/j.tplants.2015.06.008

Khatun, M., Matsushima, D., Rhaman, M. S., Okuma, E., Nakamura, T., Nakamura, Y., Munemasa, S., & Murata, Y. (2020). Exogenous proline enhances antioxidant enzyme activities but does not mitigate growth inhibition by selenate stress in tobacco BY-2 cells. *Bioscience, Biotechnology and Biochemistry*, *84*(11), 2281–2292. https://doi.org/10.1080/09168451.2020.1799747

Kitamura, A., Oasa, S., Kawaguchi, H., Osaka, M., Vukojević, V., & Kinjo, M. (2023). Increased intracellular crowding during hyperosmotic stress. *Scientific Reports*, *13*(1). https://doi.org/10.1038/s41598-023-39090-w

Kong, L., Feng, B., Yan, Y., Zhang, C., Kim, J. H., Xu, L., Rack, J. G. M., Wang, Y., Jang, J.-C., Ahel, I., Shan, L., & He, P. (2021). Noncanonical mono(ADP-ribosyl)ation of zinc finger SZF proteins counteracts ubiquitination for protein homeostasis in plant immunity. *Molecular Cell*, *81*(22), 4591-4604.e8. https://doi.org/https://doi.org/10.1016/j.molcel.2021.09.006

Koveal, D., Díaz-García, C. M., & Yellen, G. (2020). Fluorescent Biosensors for Neuronal Metabolism and the Challenges of Quantitation. *Current Opinion in Neurobiology*, *63*, 111–121. https://doi.org/https://doi.org/10.1016/j.conb.2020.02.011

Kurusu, T., Yamanaka, T., Nakano, M., Takiguchi, A., Ogasawara, Y., Hayashi, T., Iida, K., Hanamata, S., Shinozaki, K., Iida, H., & Kuchitsu, K. (2012). Involvement of the putative Ca 2+-permeable mechanosensitive channels, NtMCA1 and NtMCA2, in Ca 2+ uptake, Ca 2+-dependent cell proliferation and mechanical stress-induced gene expression in tobacco (Nicotiana tabacum) BY-2 cells. *Journal of Plant Research*, *125*(4), 555–568. https://doi.org/10.1007/s10265-011-0462-6

Kwapiszewska, K., Szczepański, K., Kalwarczyk, T., Michalska, B., Patalas-Krawczyk, P., Szymański, J., Andryszewski, T., Iwan, M., Duszyński, J., & Hołyst, R. (2020). Nanoscale Viscosity of Cytoplasm Is Conserved in Human Cell Lines. *Journal of Physical Chemistry Letters*, *11*(16), 6914–6920. https://doi.org/10.1021/acs.jpclett.0c01748

Lamport, D. T. A., Kieliszewski, M. J., & Showalter, A. M. (2006). Salt stress upregulates periplasmic arabinogalactan proteins: using salt stress to analyse AGP function*. *New Phytologist*, *169*(3), 479–492. https://doi.org/https://doi.org/10.1111/j.1469-8137.2005.01591.x

Li, J., & Yang, Y. (2023). How do plants maintain pH and ion homeostasis under saline-alkali stress? *Frontiers in Plant Science*, *14*. https://doi.org/10.3389/fpls.2023.1217193

Lintilhac, P. M., Wei, C., Tanguay, J. J., & Outwater, J. O. (2000). Ball Tonometry: A Rapid, Nondestructive Method for Measuring Cell Turgor Pressure in Thin-Walled Plant Cells. *Journal of Plant Growth Regulation*, *19*(1), 90–97. https://doi.org/10.1007/s003440000009

Liu, B., Poolman, B., & Boersma, A. J. (2017). Ionic Strength Sensing in Living Cells. *ACS Chemical Biology*, *12*(10), 2510–2514. https://doi.org/10.1021/acschembio.7b00348

Margueritat, J., Virgone-Carlotta, A., Monnier, S., Delanoë-Ayari, H., Mertani, H. C., Berthelot, A., Martinet, Q., Dagany, X., Rivière, C., Rieu, J.-P., & Dehoux, T. (2019). High-Frequency Mechanical Properties of Tumors Measured by Brillouin Light Scattering. *Physical Review Letters*, *122*(1), 18101. https://doi.org/10.1103/PhysRevLett.122.018101

Mattana, S., Mattarelli, M., Urbanelli, L., Sagini, K., Emiliani, C., Serra, M. D., Fioretto, D., & Caponi, S. (2018). Non-contact mechanical and chemical analysis of single living cells by microspectroscopic techniques. *Light: Science & Applications*, *7*(2), 17139. https://doi.org/10.1038/lsa.2017.139

Maurel, C., Tacnet, F., Gu¨clu¨*, J., Gu¨clu¨*, G., Guern, J., & Ripoche, P. (1997). Purified vesicles of tobacco cell vacuolar and plasma membranes exhibit dramatically different water permeability and water channel activity. In *Plant Biology* (Vol. 94).

McKenna, J. F., Rolfe, D. J., Webb, S. E. D., Tolmie, A. F., Botchway, S. W., Martin-Fernandez, M. L., Hawes, C., & Runions, J. (2019). The cell wall regulates dynamics and size of plasma-membrane nanodomains in Arabidopsis. *Proceedings of the National Academy of Sciences of the United States of America*, *116*(26), 12857–12862. https://doi.org/10.1073/pnas.1819077116

Michels, L., Gorelova, V., Harnvanichvech, Y., Borst, J. W., Albada, B., Weijers, D., & Sprakel, J. (2020). Complete microviscosity maps of living plant cells and tissues with a toolbox of targeting mechanoprobes. *Proceedings of the National Academy of Sciences of the United States of America*, *117*(30), 18110–18118. https://doi.org/10.1073/pnas.1921374117

Milani, P., Gholamirad, M., Traas, J., Arnéodo, A., Boudaoud, A., Argoul, F., & Hamant, O. (2011). *In vivo* analysis of local wall stiffness at the shoot apical meristem in Arabidopsis using atomic force microscopy. *The Plant Journal*, *67*(6), 1116–1123. https://doi.org/10.1111/j.1365-313X.2011.04649.x

Miller, R. C., Aplin, C. P., Kay, T. M., Leighton, R., Libal, C., Simonet, R., Cembran, A., Heikal, A. A., Boersma, A. J., & Sheets, E. D. (2020). FRET Analysis of Ionic Strength Sensors in the Hofmeister Series of Salt Solutions Using Fluorescence Lifetime Measurements. *Journal of Physical Chemistry B*, *124*(17), 3447–3458. https://doi.org/10.1021/acs.jpcb.9b10498

Moulia, B., Bastien, R., Chauvet-Thiry, H., & Leblanc-Fournier, N. (2019). Posture control in land plants: growth, position sensing, proprioception, balance, and elasticity. *Journal of Experimental Botany*, *70*(14), 3467–3494. https://doi.org/10.1093/jxb/erz278

Moulia, B., Coutand, C., & Julien, J.-L. (2015). Mechanosensitive control of plant growth: bearing the load, sensing, transducing, and responding. *Frontiers in Plant Science*, *6*(February), 52. https://doi.org/10.3389/fpls.2015.00052

Moulia, B., Douady, S., & Hamant, O. (2021). Fluctuations shape plants through proprioception. *Science*, *372*(6540). https://doi.org/10.1126/science.abc6868

Mousavi, S. A. R., Dubin, A. E., Zeng, W. Z., Coombs, A. M., Do, K., Ghadiri, D. A., Keenan, W. T., Ge, C., Zhao, Y., & Patapoutian, A. (2021). PIEZO ion channel is required for root mechanotransduction in Arabidopsis thaliana. *Proceedings of the National Academy of Sciences of the United States of America*, *118*(20), 1–27. https://doi.org/10.1073/pnas.2102188118

Naguro, I., Umeda, T., Kobayashi, Y., Maruyama, J., Hattori, K., Shimizu, Y., Kataoka, K., Kim-Mitsuyama, S., Uchida, S., Vandewalle, A., Noguchi, T., Nishitoh, H., Matsuzawa, A., Takeda, K., & Ichijo, H. (2012). ASK3 responds to osmotic stress and regulates blood pressure by suppressing WNK1-SPAK/OSR1 signaling in the kidney. *Nature Communications*, *3*. https://doi.org/10.1038/ncomms2283

Olmos, E., De La Garma, J. G., Gomez-Jimenez, M. C., & Fernandez-Garcia, N. (2017a). Arabinogalactan proteins are involved in salt-adaptation and vesicle trafficking in tobacco by-2 cell cultures. *Frontiers in Plant Science*, *8*(June), 1–14. https://doi.org/10.3389/fpls.2017.01092

Olmos, E., De La Garma, J. G., Gomez-Jimenez, M. C., & Fernandez-Garcia, N. (2017b). Arabinogalactan proteins are involved in salt-adaptation and vesicle trafficking in tobacco by-2 cell cultures. *Frontiers in Plant Science*, *8*. https://doi.org/10.3389/fpls.2017.01092

Peaucelle, A., Braybrook, S. A., Le Guillou, L., Bron, E., Kuhlemeier, C., & Höfte, H. (2011). Pectin-Induced Changes in Cell Wall Mechanics Underlie Organ Initiation in Arabidopsis. *Current Biology*, *21*(20), 1720–1726. https://doi.org/10.1016/j.cub.2011.08.057

Persson, L. B., Ambati, V. S., & Brandman, O. (2020). Cellular Control of Viscosity Counters Changes in Temperature and Energy Availability. *Cell*, *183*(6), 1572-1585.e16. https://doi.org/10.1016/j.cell.2020.10.017

Roberts, A. B., Zhang, J., Raj Singh, V., Nikolić, M., Moeendarbary, E., Kamm, R. D., So, P. T. C., & Scarcelli, G. (2021). Tumor cell nuclei soften during transendothelial migration. *Journal of Biomechanics*, *121*, 110400. https://doi.org/10.1016/j.jbiomech.2021.110400

Robinson, M., Filice, C. T., McRae, D. M., & Leonenko, Z. (2023). Atomic force microscopy and other scanning probe microscopy methods to study nanoscale domains in model lipid membranes. *Advances in Physics: X*, *8*(1), 2197623. https://doi.org/10.1080/23746149.2023.2197623

Roffay, C., Molinard, G., Kim, K., Urbanska, M., Andrade, V., Barbarasa, V., Nowak, P., Mercier, V., García-Calvo, J., Matile, S., Loewith, R., Echard, A., Guck, J., Lenz, M., & Roux, A. (2021). Passive coupling of membrane tension and cell volume during active response of cells to osmosis. *BIOPHYSICS AND COMPUTATIONAL BIOLOGY CELL BIOLOGY*. https://doi.org/10.1073/pnas.2103228118/-/DCSupplemental

Romero-Perez, P. S., Dorone, Y., Flores, E., Sukenik, S., & Boeynaems, S. (2023). When Phased without Water: Biophysics of Cellular Desiccation, from Biomolecules to Condensates. In *Chemical Reviews* (Vol. 123, Issue 14, pp. 9010–9035). American Chemical Society. https://doi.org/10.1021/acs.chemrev.2c00659

Routier-Kierzkowska, A.-L., Weber, A., Kochova, P., Felekis, D., Nelson, B. J., Kuhlemeier, C., & Smith, R. S. (2012). Cellular Force Microscopy for in Vivo Measurements of Plant Tissue Mechanics . *Plant Physiology*, *158*(4), 1514–1522. https://doi.org/10.1104/pp.111.191460

Sampathkumar, A., Krupinski, P., Wightman, R., Milani, P., Berquand, A., Boudaoud, A., Hamant, O., Jönsson, H., & Meyerowitz, E. M. (2014). Subcellular and supracellular mechanical stress

prescribes cytoskeleton behavior in Arabidopsis cotyledon pavement cells. *ELife*, *3*. https://doi.org/10.7554/eLife.01967

Seelbinder, B., Wagner, S., Jain, M., Erben, E., Klykov, S., Stoev, I. D., Krishnaswamy, V. R., & Kreysing, M. (2024). Probe-free optical chromatin deformation and measurement of differential mechanical properties in the nucleus. *ELife*, *13*. https://doi.org/10.7554/eLife.76421

Skrzypczak, T., Wojtaszek, P., & Kasprowicz-Maluśki, A. (2024). Heterogenous transcriptomes of Nicotiana tabacum BY-2 suspension cell lines adapted to various osmoticum. *Biorxiv.Org*. https://doi.org/10.1101/2024.04.24.590873

Srba, M., Černíková, A., Opatrný, Z., & Fischer, L. (2016). Practical guidelines for the characterization of tobacco BY-2 cell lines. *Biologia Plantarum*, *60*(1), 13–24. https://doi.org/10.1007/s10535-015-0573-3

Steinbeck, J., Fuchs, P., Negroni, Y. L., Elsässer, M., Lichtenauer, S., Stockdreher, Y., Feitosa-Araujo, E., Kroll, J. B., Niemeier, J.-O., Humberg, C., Smith, E. N., Mai, M., Nunes-Nesi, A., Meyer, A. J., Zottini, M., Morgan, B., Wagner, S., & Schwarzländer, M. (2020). In Vivo NADH/NAD+ Biosensing Reveals the Dynamics of Cytosolic Redox Metabolism in Plants. *The Plant Cell*, *32*(10), 3324–3345. https://doi.org/10.1105/tpc.20.00241

Tanaka, H. (2022). Viscoelastic phase separation in biological cells. *Communications Physics*, *5*(1). https://doi.org/10.1038/s42005-022-00947-7

Tomos, A. D., & Leigh, R. A. (1999). THE PRESSURE PROBE: A Versatile Tool in Plant Cell Physiology. *Annual Review of Plant Physiology and Plant Molecular Biology*, *50*(1), 447–472. https://doi.org/10.1146/annurev.arplant.50.1.447

Trinh, D.-C., Alonso-Serra, J., Asaoka, M., Colin, L., Cortes, M., Malivert, A., Takatani, S., Zhao, F., Traas, J., Trehin, C., & Hamant, O. (2021). How Mechanical Forces Shape Plant Organs. *Current Biology*, *31*(3), R143–R159. https://doi.org/10.1016/j.cub.2020.12.001

Uribe, S., & Sampedro, J. G. (2003). Measuring solution viscosity and its effect on enzyme activity. *Biological Procedures Online*, *5*(1), 108–115. https://doi.org/10.1251/bpo52

van der Linden, F. H., Mahlandt, E. K., Arts, J. J. G., Beumer, J., Puschhof, J., de Man, S. M. A., Chertkova, A. O., Ponsioen, B., Clevers, H., van Buul, J. D., Postma, M., Gadella, T. W. J., & Goedhart, J. (2021). A turquoise fluorescence lifetime-based biosensor for quantitative imaging of intracellular calcium. *Nature Communications*, *12*(1), 7159. https://doi.org/10.1038/s41467-021-27249-w

van Zelm, E., Zhang, Y., & Testerink, C. (2020). Salt Tolerance Mechanisms of Plants. *Annual Review of Plant Biology*, *71*, 403–433. https://doi.org/10.1146/annurev-arplant-050718-100005

WANG, C. X. (2004). Modelling the Mechanical Properties of Single Suspension-Cultured Tomato Cells. *Annals of Botany*, *93*(4), 443–453. https://doi.org/10.1093/aob/mch062

Wang, L., Hukin, D., Pritchard, J., & Thomas, C. (2006). Comparison of plant cell turgor pressure measurement by pressure probe and micromanipulation. *Biotechnology Letters*, *28*(15), 1147–1150. https://doi.org/10.1007/s10529-006-9075-x

Watanabe, K., Morishita, K., Zhou, X., Shiizaki, S., Uchiyama, Y., Koike, M., Naguro, I., & Ichijo, H. (2021). Cells recognize osmotic stress through liquid–liquid phase separation lubricated with poly(ADP-ribose). *Nature Communications*, *12*(1). https://doi.org/10.1038/s41467-021-21614-5

Watson, J. L., Seinkmane, E., Styles, C. T., Mihut, A., Krüger, L. K., McNally, K. E., Planelles-Herrero, V. J., Dudek, M., McCall, P. M., Barbiero, S., Vanden Oever, M., Peak-Chew, S. Y., Porebski, B. T., Zeng, A., Rzechorzek, N. M., Wong, D. C. S., Beale, A. D., Stangherlin, A., Riggi, M., … Derivery, E. (2023a). Macromolecular condensation buffers intracellular water potential. *Nature*. https://doi.org/10.1038/s41586-023-06626-z

Watson, J. L., Seinkmane, E., Styles, C. T., Mihut, A., Krüger, L. K., McNally, K. E., Planelles-Herrero, V. J., Dudek, M., McCall, P. M., Barbiero, S., Vanden Oever, M., Peak-Chew, S. Y., Porebski, B. T., Zeng, A., Rzechorzek, N. M., Wong, D. C. S., Beale, A. D., Stangherlin, A., Riggi, M., … Derivery, E. (2023b). Macromolecular condensation buffers intracellular water potential. *Nature*. https://doi.org/10.1038/s41586-023-06626-z

Weber, A., Braybrook, S., Huflejt, M., Mosca, G., Routier-Kierzkowska, A. L., & Smith, R. S. (2015). Measuring the mechanical properties of plant cells by combining micro-indentation with osmotic treatments. *Journal of Experimental Botany*, *66*(11), 3229–3241. https://doi.org/10.1093/jxb/erv135

Wisniewski, E. O., Mistriotis, P., Bera, K., Law, R. A., Zhang, J., Nikolic, M., Weiger, M., Parlani, M., Tuntithavornwat, S., Afthinos, A., Zhao, R., Wirtz, D., Kalab, P., Scarcelli, G., Friedl, P., & Konstantopoulos, K. (2020). Dorsoventral polarity directs cell responses to migration track geometries. *Science Advances*, *6*(31). https://doi.org/10.1126/sciadv.aba6505

Wu, P. J., Kabakova, I. V., Ruberti, J. W., Sherwood, J. M., Dunlop, I. E., Paterson, C., Török, P., & Overby, D. R. (2018). Water content, not stiffness, dominates Brillouin spectroscopy measurements in hydrated materials. In *Nature Methods* (Vol. 15, Issue 8, pp. 561–562). Nature Publishing Group. https://doi.org/10.1038/s41592-018-0076-1

Wu, P.-H., Aroush, D. R.-B., Asnacios, A., Chen, W.-C., Dokukin, M. E., Doss, B. L., Durand-Smet, P., Ekpenyong, A., Guck, J., Guz, N. V, Janmey, P. A., Lee, J. S. H., Moore, N. M., Ott, A., Poh, Y.-C., Ros, R., Sander, M., Sokolov, I., Staunton, J. R., … Wirtz, D. (2018). A comparison of methods to assess cell mechanical properties. *Nature Methods*, *15*(7), 491–498. https://doi.org/10.1038/s41592-018-0015-1

Yan, G., Monnier, S., Mouelhi, M., & Dehoux, T. (2021). Probing molecular crowding in compressed tissues with Brillouin light scattering. *BIOPHYSICS AND COMPUTATIONAL BIOLOGY*. https://doi.org/10.1073/pnas.2113614119/-/DCSupplemental

Yao, D., Arguez, M. A., He, P., Bent, A. F., & Song, J. (2021). Coordinated regulation of plant immunity by poly(ADP-ribosyl)ation and K63-linked ubiquitination. *Molecular Plant*, *14*(12), 2088–2103. https://doi.org/https://doi.org/10.1016/j.molp.2021.08.013

Zamora-Briseño, J. A., Pereira-Santana, A., Reyes-Hernández, S. J., Cerqueda-García, D., Castaño, E., & Rodríguez-Zapata, L. C. (2021). Towards an understanding of the role of intrinsic protein disorder on plant adaptation to environmental challenges. *Cell Stress and Chaperones*, *26*(1), 141–150. https://doi.org/https://doi.org/10.1007/s12192-020-01162-5

Zhang, J., Nikolic, M., Tanner, K., & Scarcelli, G. (2023). Rapid biomechanical imaging at low irradiation level via dual line-scanning Brillouin microscopy. *Nature Methods*, *20*(5), 677–681. https://doi.org/10.1038/s41592-023-01816-z

Zhao, C., Zhang, H., Song, C., Zhu, J. K., & Shabala, S. (2020). Mechanisms of Plant Responses and Adaptation to Soil Salinity. *The Innovation*, *1*(1), 100017. https://doi.org/10.1016/j.xinn.2020.100017

Zhu, J. K. (2002). Salt and drought stress signal transduction in plants. *Annual Review of Plant Biology*, *53*, 247–273. https://doi.org/10.1146/annurev.arplant.53.091401.143329

Zonia, L., & Munnik, T. (2007). Life under pressure: hydrostatic pressure in cell growth and function. *Trends in Plant Science*, *12*(3), 90–97. https://doi.org/10.1016/j.tplants.2007.01.006

Zwiewka, M., Nodzyński, T., Robert, S., Vanneste, S., & Friml, J. (2015). Osmotic Stress Modulates the Balance between Exocytosis and Clathrin-Mediated Endocytosis in Arabidopsis thaliana. *Molecular Plant*, *8*(8), 1175–1187. https://doi.org/10.1016/j.molp.2015.03.007